Articulo publicado en CHEMICAL ENGINEERING JOURNAL
Vol. 393, Pags. 124775 1-18

Conventional and improved fluidized bed reactors for dry reforming of methane: Mathematical models

Zambrano, D.; Soler, J.; Herguido, J.; Menéndez, M.

DOI: https://doi.org/10.1016/j.cej.2020.124775

Conventional and improved fluidized bed reactors for dry reforming of methane: mathematical models

D. Zambrano, J. Soler, J. Herguido, M. Menéndez*

Department of Chemical and Environmental Engineering. I3A- University of Zaragoza. Spain

*Miguel.menendez@unizar.es

Keywords: Dry reforming of methane; two-zone fluidized bed reactor; Pd membrane; membrane reactor; pure hydrogen production

Abstract

Dry reforming of methane is a potentially useful reaction, but has some drawbacks: catalyst deactivation by coke and yield limited by thermodynamic equilibrium. New improved fluidized bed reactors may compensate these disadvantages. Mathematical models for the dry reforming of methane in three types of fluidized bed reactors have been developed. These reactors include: a) conventional fluidized bed reactor, b) two zone fluidized bed reactor, which provides simultaneous reaction and catalyst regeneration in a single fluidized bed, and c) two-zone fluidized bed reactor with hydrogen selective membranes, which in addition to the previous one provides increased yield to hydrogen, because the selective removal of hydrogen through the membrane. The situations where these reactors counteract the two main drawbacks of dry reforming of methane are shown. Comparison with previous experimental results shows that the models predict well the effect of operating conditions.

1 Introduction

Dry reforming of methane (DRM) allows the production of hydrogen from carbon dioxide and methane according to the following reaction:

$$CH_4 + CO_2 \longleftrightarrow 2H_2 + 2CO \qquad \text{(r.1)}$$

In addition to the main reaction (r.1), several other reactions should be considered for a suitable description of the process kinetics [1]:

- Reverse water-gas-shift

$$CO_2 + H_2 \longleftrightarrow CO + H_2O \qquad \text{(r.2)}$$

- Boudouard reaction

$$2CO \longleftrightarrow C_{(s)} + CO_2 \qquad \text{(r.3)}$$

- Methane decomposition

$$CH_4 \longleftrightarrow C_{(s)} + 2H_2 \qquad \text{(r.4)}$$

- Reverse of carbon gasification by water

$$CO + H_2 \longleftrightarrow C_{(s)} + H_2O \qquad \text{(r.5)}$$

DRM is an alternative to the conventional process of steam reforming of methane (SRM), industrially employed to obtain synthesis gas or H_2 . DRM has some advantages over SRM:

-DRM allows simultaneously upgrading the two gases found in the biogas. This biogas is obtained by the fermentation of organic wastes, and therefore it can be a renewable energy source.

- DRM prevents the emission into the atmosphere of these two gases, which are greenhouse gases.

- DRM provides an H_2/CO ratio close to 1, which may be interesting in some processes.

The DRM studies can be traced back to Fischer and Tropsch [2] end even earlier publications dated in 1888 [3]. However this reaction has not been the basis of hydrogen or syngas production in industrial practice, probably due to the catalyst deactivation by coke. In fact, cofeeding some CO_2 in SRM is a usual industrial practice, in order to reduce the H_2/CO ratio, but there are not industrial processes based only on DRM.

Interest in the DRM reaction has grown in recent years, as evidenced by numerous reviews [4-8]. The problem of deactivation by coke has not been solved, which would require the use of packed bed reactors with cycles of operation and regeneration, or systems with circulation between the reactor and regenerator, as proposed by Prasad and Elnashaie [9] , similar to the circulating fluidized bed of the FCC process.

Another alternative to solve this problem is the use of the two-zone fluidized bed reactor (TZFBR). The scheme of this type of reactor is shown in Figure 1b, where the difference with a conventional fluidized bed rector (Figure 1a) is shown. This type of reactor has two zones with different atmospheres, created by means of two feeds, one at the bottom of a fluidized bed and the other at an intermediate point of the bed. In this way, one reaction can be carried out at the upper zone and another at the lower zone. This reactor has been used in several processes with deactivation by coke formation [10, 11]. In those cases, the desired reaction occurs in the upper zone of the bed, while coke is deposited on the catalyst. In the lower zone of the bed an oxidizing gas (oxygen, carbon dioxide or water) reacts with the coke coming from the upper zone, regenerating the catalyst. Being a fluidized bed, there is an intense mixing of solid, which causes the transport of the catalyst between the two zones. In addition, the transport of solid helps to keep a good isothermicity of the bed [12]. Under suitable operating conditions the catalyst can be regenerated at the same time that the reaction is being carried out, whereby we have an example of process intensification, by carrying out two reactions, the desired main reaction and regeneration, in the same reactor. Previous works showed experimentally that TZFBR may operate with a high degree of isothermicity [12] and that it is possible to avoid the presence of oxygen in the upper zone [12, 13]. Other experiments showed that the performance of this reactor can be scaled-up [14,15].

A further improvement on the TZFBR is the use of membranes, to selectively remove one of the reaction products. Hydrogen selective membranes have been employed in fluidized bed reactors by several groups [16-21] and recent develpments show steady use for long time [22] and that new, attrition resistant membranes have been developed [23]. Although membrane reactors have been widely studied, their application with TZFBR is quite new. This configuration, named TZFBR+MB is shown in Figure 1c. It was firstly employed in propane dehydrogenation [24, 25].

Previous work has shown that it is possible to use a TZFBR for DRM. Ugarte et al. [26] showed that constant performance can be maintained along the time-on-stream in a TZFBR, while this was not possible in a conventional fluidized bed reactor. They also showed that it was possible to introduce hydrogen selective membranes in a TZFBR for DRM. Durán et al. [27] showed that using a suitable ratio of membrane area to catalyst weight the hydrogen yield can be increased by 100-200%, and in addition most of it is

obtained as high purity hydrogen, because it has permeated through the palladium membrane.

The TZFBR+MB implies a high degree of process intensification since we are carrying out two reactions in the same reactor, both the desired reaction and the regeneration of the catalyst, and simultaneously the separation of the desired product.

It should be mentioned that in many cases, when hydrogen selective membrane are used in membrane reactors to remove hydrogen from the reaction medium, the deactivation rate due to coke formation increases, which is a serious inconvenience [28-30]. In this case, having a TZFBR allows hydrogen to be extracted, compensating the additional catalyst deactivation by *in situ* catalyst regeneration.

In some previous works, the mathematical modeling of two-zone fluidized bed reactors has been addressed [31-32]. However, no mathematical model for DRM in a TZFBR has yet been published, neither the modeling of a TZFBR+MB has been previously addressed.

This work aims to develop this mathematical model, both for the TZFBR and for the TZFBR+MB. The results obtained will be compared with the experimental results presented in the previous works [26, 27] and some new results in CFBR.

2 Experimental system.

Although this work is mainly about mathematical modeling of reactor, it includes unpublished experimental results in conventional fluidized bed reactor. The experiments were made in the same experimental systems previously described [26, 27]. It includes a quartz reactor 3 cm diameter, with a porous plate as gas distributor and on-line analysis by gas chromatography. The catalyst is Ni-Ce/Al_2O_3 catalyst, already described [26]. It contains 5% Ni and 10% Ce by weight and was prepared by incipient wetness method on a fluidizable alumina (Sasol- Puralox ® SCCa-150/200). The Pd-Ag membranes with a total length of 15.2 cm, external diameter of 0.32 cm and a thickness of the Pd/Ag layer of 76 μm, were supplied by Reb Research. One experiment was repeated several times along 50 hours of total time-on-stream and the standard deviation of the mean conversion was 0,6 percentage points

3. Mathematical models.

The mathematical models are based on previous proposals for TZFBR. Soler et al. [31] proposed a model with constant bubble size for the study of oxidative dehydrogenation of n-butane in a TZFBR. Rubio et al. [32] studied the same process in

an Interconnected Fluidized Bed Reactor with Internal Circulation (ICFBR), improving the model proposed by Soler et al. [31] by considering a variable bubble size with the bed height. Gascón et al. [33] evaluated the latter model in the dehydrogenation of propane and the partial oxidation of n-butane, using both TZFBR and ICFBR configurations.

3.1. Gas and solid flow models

The gas flow model mainly follows the description of the three-phase model proposed by Kunii and Levenspiel [34]. This model considers that the bed is divided into three phases: bubble, emulsion and cloud (Figure 2).

The gas is considered to rise in the emulsion at a relative speed roughly equal to the minimum fluidization rate ($u_e \approx u_{mf}$), while the remaining gas rises with the bubbles at a rate u_b.

According to the fast bubble model proposed by Davidson and Harrison [35], most of the gas inside the bubble is continuously being recirculated, penetrating only slightly into the emulsion. The gas that is circulating around the bubble forms the cloud. The bubble carries a certain amount of solid in its upward movement, called the wake.

Therefore, it is considered that the bubbles drag solid in the wake, when ascending through the bed. Exchange rate of solid between the rising wake and the surrounding emulsion is characterized by an exchange coefficient K_{we}. Once a bubble reaches the surface of the bed, the solid passes into the emulsion and descends.

Due to the continuous recirculation of the gas inside the bubble, the same concentration of the gas in the bubble and in the wake is considered. In addition, the gas transfer between the cloud and the emulsion is much faster than between the bubble and the cloud, therefore, the same concentration of gas for the cloud and the emulsion is also considered.

Also, some additional assumptions were made in the development of the model:

- Isothermal bed, due to the high degree of solid mixing.
- The gas velocity in the emulsion ($u_e \approx u_{mf}$) and the porosity (ε_{mf}) in the emulsion phase are those measured experimentally under conditions of minimum fluidization.
- For TZFBR and TZFBR + MB, the reactant gas (CH_4 + CO_2) is instantly mixed at the supply point (h_f) with inert (N_2/Ar) and regenerating gas (O_2/CO_2) stream arriving from the lower zone. Thus, the reactant is distributed proportionally between the bubble phase and the emulsion phase. This assumption was previously made in models developed by our group [32,33], since it provided a

better fit to the experimental results than when we assumed that the reactant gas only forms new bubbles.

The equations used to estimate the bubble size (d_b), the bubble rise velocity (u_b), the gas exchange coefficient between bubble and emulsion (K_{be}), the coefficient of solids exchange between wake and emulsion (K_{we}) and other parameters that appear in the fluid dynamic model are shown in Table 1.

The minimum fluidization rate (u_{mf}) and the minimum fluidization porosity (ε_{mf}) have been determined experimentally. For the volumetric fraction of the wake in the bubbles (f_w) a value of 0.15 was considered as stated by Gascón et al. [33]. For the calculation of the bubble diameter (d_b) and the initial bubble diameter (d_{bo}) in the CFBR, the equations proposed by Mori and Wen [36] were used, while the bubble rise rate (u_b) was calculated by the expression used by Kunii and Levenspiel [37]. For the TZFBR and the TZFBR + MB the bubble size (d_b) was estimated using the JHM correlation proposed by Julián et al. [38].

As for the flow model for the solid species, the solid present in the wake rises at the same speed as the bubbles, while the solid that is in the emulsion drops at a speed u_s, such that upward and downward solid flows equalize. The gas exchange coefficients between the bubble phase and the emulsion phase (K_{be}, K_{bc}, K_{ce}) and the solid exchange coefficient (K_{we}) between the wake phase and the emulsion phase were calculated according to the expressions proposed by Kunii and Levenspiel [39].

The kinetic models of the chemical reactions must be added, to complete the mathematical model, both those concerning the gas phase and the solid phase. In addition, depending on the configuration of the reactor, the kinetic models of coke combustion (with O_2) or gasification (with CO_2) and the model for H_2 permeation through the membrane will be added.

Table 1 Equations employed in the fluid-dynamics model

Bubble diameter	
CFBR [36, 40]	
$d_{b0} = 3.77\left(u_{sg} - u_{mf}\right)^2 g^{-1}$	(1)
$d_{bm} = 1.49 g^{-0.2}\left[\pi D_i^2 \left(u_{sg} - u_{mf}\right)\right]^{0.4}$	(2)
$d_b = d_{bm} - \left(d_{bm} - d_{b0}\right)\exp\left(-\frac{0.3H}{D_i}\right)$	(3)
TZFBR/TZFBR + MB (JHM correlation by Julián et al. [38])	
- Regeneration zone ($H < h_f$)	
$d_{bo,1} = 3.77\left(u_{sg,1} - u_{mf}\right)^2 g^{-1}$	(4)
$d_{bm,1} = 1.49 g^{-0.2}\left[\pi D_i^2 \left(u_{sg1} - u_{mf}\right)\right]^{0.4}$	(5)

$$d_{b,1} = d_{bm,1} - \left(d_{bm,1} - d_{bo}\right)\exp\left(-\frac{0.3H}{D_i}\right) \quad (6)$$

- Reaction zone ($H > h_f$)

$$d_{bo,2} = d_{b,1}(H = h_f) \quad (7)$$

$$d_{bm,2} = 1.49 g^{-0.2}\left[\pi D_i^2\left(u_{sg2} - u_{mf}\right)\right]^{0.4} \quad (8)$$

$$d_{b,2} = d_{bm,2} - \left(d_{bm,2} - d_{bo,2}\right)\exp\left(-\frac{0.3H}{D_i}\right) \quad (9)$$

$$d_{b,orif} = d_{bm,2} - \left(d_{bm,2} - d_{orif}\right)\exp\left(-\frac{0.3H}{D_i}\right) \quad (10)$$

$$d_b = \frac{d_{b,2}^3 + d_{b,orif}^3}{d_{b,2}^2 + d_{b,orif}^2} \quad (11)$$

Bubble rise velocity [37, ,40]

$$u_b = \left(u_{sg} - u_{mf}\right) + 0.711\left(g d_b\right)^{0.5} \quad (12)$$

Bubble-emulsion gas Exchange coefficients [39, 40]

$$K_{bc} = 4.5\left(\frac{u_{mf}}{d_b}\right) + 5.85\left(\frac{D_{jm}^{0.5} g^{0.25}}{d_b^{5/4}}\right) \quad (13)$$

$$K_{ce} = 6.78\left(\frac{\varepsilon_{mf} D_{jm} u_b}{d_b^3}\right)^{0.5} \quad (14)$$

$$\frac{1}{K_{be}} \approx \frac{1}{K_{bc}} + \frac{1}{K_{ce}} \quad (15)$$

$$D_{jm} = \left(\sum_{\substack{i=1 \\ i \neq j}} \frac{y_i}{D_{ij}}\right)^{-1} \quad (16)$$

$$D_{ij} = 1.858 \times 10^{-3} T^{3/2} \frac{\left(\frac{M_i + M_j}{M_i M_j}\right)^{0.5}}{P\sigma_{ij}^2 \Omega_{ij}} \quad (17)$$

$$\sigma_{ij} = \frac{\sigma_i + \sigma_j}{2} \quad (18)$$

$$\sigma_j = \frac{2.3551 - 0.087\omega_j}{\left(\frac{P_{c,j}}{T_{c,j}}\right)^{\frac{1}{3}}} \quad (19)$$

$$\Omega_{ij} = \frac{A}{\left(T_{ij}^*\right)^B} + \frac{C}{\exp\left(DT_{ij}^*\right)} + \frac{E}{\exp\left(FT_{ij}^*\right)} + \frac{G}{\exp\left(HT_{ij}^*\right)} \quad (20)$$

$$T_{ij}^* = \frac{kT}{\varepsilon_{ij}} \quad (21)$$

$$\frac{\varepsilon_j}{kT_{c,j}} = 0.7915 + 0.1693\omega_j \quad (22)$$

Wake-emulsion solid Exchange coefficients [39,40]

$$K_{we} = \frac{0.075\left(u_{sg} - u_{mf}\right)}{u_{mf} d_b} \text{ if } \frac{u_{sg}}{u_{mf}} \leq 3 \quad (23)$$

$$K_{we} = \frac{0.15}{d_b} \text{ if } \frac{u_{sg}}{u_{mf}} > 3 \quad (24)$$

Volume fractions [40]

$$\delta = \frac{u_{sg} - u_{mf}}{u_b - u_{mf} - u_{mf} f_w} \quad (25)$$

$$u_s = \frac{\delta f_w u_b}{1 - \delta - \delta f_w} \quad (26)$$

$$u_e = \frac{u_{mf}}{\varepsilon_{mf}} - u_s \quad (27)$$

3.2 Kinetic models.

The kinetic model includes the three reactions previously described (r.1-DRM, r.2-reverse water gas shift and r.3-Boudouard reaction). The kinetics for these reaction is described by Langmuir-Hinshelwood-Hougen-Watson models, as found by Zambrano et al. [1]. In addition, two reactions are included to account for coke formation (r.4-methane decomposition and r.5-reverse of carbon gasification by water). This model was obtained in a temperature range between 475 ℃ and 550 ℃, the molar ratio of reactants (CH_4/CO_2)in the feed was between 0.6 and 1.67 and the methane conversion between approximately 7% and 33%.

The catalyst deactivation rate was described by

$$-\frac{da}{dt} = \varphi_d a^d - \varphi_r \quad (28)$$

$$\varphi_d = \frac{k_{d1} P_{CH_4}^2 + k_{d2} P_{H_2}^2 P_{CO}^2}{\left(1 + k_{d3} P_{CO_2}\right)^2} \quad (29)$$

$$\varphi_r = k_{r1} P_{CO_2}^2 \quad (30)$$

And the relationship between coke content and catalyst activity is:

$$a = \left(1 - \frac{C_c}{C_{cmax}}\right)^2 \quad (31)$$

When oxygen is employed for the regeneration, the reaction rate for coke combustion is given by:

$$-\frac{dC_c}{dt} = l_a k_a^{\dagger} P_{O_2} \frac{\left(C_{ca}/C_{coa}\right)^{1/3}}{1-\left(C_{ca}/C_{coa}\right)^{1/3}} + l_g k_g^{\dagger} P_{O_2} \left(C_{cg}/C_{cog}\right)^{3} \quad (32)$$

And when CO_2 is employed, the reaction rate between coke and CO_2 is given by:

$$-\frac{dC_c}{dt} = l_a k_a^{\dagger} P_{CO_2} \frac{\left(C_{ca}/C_{coa}\right)^{5/3}}{1-\left(C_{ca}/C_{coa}\right)^{1/3}} + l_g k_g^{\dagger} P_{CO_2} \frac{\left(C_{cg}/C_{cog}\right)^{5/3}}{1-\left(C_{cg}/C_{cog}\right)^{1/3}} \quad (33)$$

3.3 Mass balances.

From the above described fluid dynamic models for the gas and for the solid, the mass balances in non-steady state were made in a differential reactor volume element. In each volume element (Figure 3) the mass balance is:

Accumulation = In - Out ± Transfer ± Reaction (34)

With the mass balance, applying the proposed flow model, the following partial differential equations are obtained in a dimension (z) for a CFBR:

Mass balance for the gas phase

Phase: Bubble (b) + Wake (w) (35)

$$\left(\delta + \delta f_w \varepsilon_{mf}\right)\frac{\partial C_{i,b}}{\partial t} = -\frac{\partial\left(\left(\delta + \delta f_w \varepsilon_{mf}\right) u_b C_{i,b}\right)}{\partial z} + \left(\lambda_1 C_{i,b} + \lambda_2 C_{i,e}\right)\frac{\partial\left(\left(\delta + \delta f_w \varepsilon_{mf}\right) u_b\right)}{\partial z} - K_{b,e}\left(\delta + \delta f_w \varepsilon_{mf}\right)\left(C_{i,b} - C_{i,e}\right) + r_{i,b}\rho_{cat}\left(1-\varepsilon_{mf}\right)\delta f_w$$

Phase: Emulsion (e) (36)

$$\left(1-\delta-\delta f_w\right)\varepsilon_{mf}\frac{\partial C_{i,e}}{\partial t} = -\frac{\partial\left(\left(1-\delta-\delta f_w\right)\varepsilon_{mf} u_e C_{i,e}\right)}{\partial z} - \left(\lambda_1 C_{i,b} + \lambda_2 C_{i,e}\right)\frac{\partial\left(\left(\delta + \delta f_w \varepsilon_{mf}\right) u_b\right)}{\partial z}$$

$$+ K_{b,e}\left(\delta + \delta f_w \varepsilon_{mf}\right)\left(C_{i,b} - C_{i,e}\right)$$

$$+ r_{i,e}\rho_{cat}\left(1-\delta-\delta f_w\right)\left(1-\varepsilon_{mf}\right)$$

Mass balance for the solid phase

Phase: Wake (w) (37)

$$\left(1-\varepsilon_{mf}\right)\delta f_w \frac{\partial C_{j,w}}{\partial t} = -\frac{\partial\left(\left(1-\varepsilon_{mf}\right)\delta f_w u_b C_{j,w}\right)}{\partial z} + \left(\lambda_1 C_{j,w} + \lambda_2 C_{j,e}\right)\frac{\partial\left(\left(1-\varepsilon_{mf}\right)\delta f_w u_b\right)}{\partial z} - K_{w,e}\left(1-\varepsilon_{mf}\right)\delta f_w\left(C_{j,w} - C_{j,e}\right) + r_{j,w}\left(1-\varepsilon_{mf}\right)\delta f_w$$

Phase: Emulsion (e) (38)

$$\left(1-\varepsilon_{mf}\right)\left(1-\delta-\delta f_w\right)\frac{\partial C_{j,e}}{\partial t} = -\frac{\partial\left(\left(1-\varepsilon_{mf}\right)\left(1-\delta-\delta f_w\right)u_s C_{j,e}\right)}{\partial z} - \left(\lambda_1 C_{j,w} + \lambda_2 C_{j,e}\right)\frac{\partial\left(\left(1-\varepsilon_{mf}\right)\delta f_w u_b\right)}{\partial z} + K_{w,e}\left(1-\varepsilon_{mf}\right)\delta f_w\left(C_{j,w} - C_{j,e}\right) + r_{j,e}\left(1-\varepsilon_{mf}\right)\left(1-\delta-\delta f_w\right)$$

Transversal flow (second term in the r.h.s. of eq. 37 and eq. 38) is a consequence from the variation of bubble properties with height [41–43]. The fraction of bed volume occupied by bubbles changes along the bed height, because their size and speed change. Thus, the distribution of the gas flow between the bubble and emulsion phases also changes. A change in the volumetric flow rate of the bubble must be compensated with a net flow of gas or solid, either from the emulsion to the bubble - wake or vice versa.

The term that takes into account the transversal flow (i.e. flow of solid between wake and emulsion because the change of bubble properties) has the following form:

$$\left(\lambda_1 C_{x,y} + \lambda_2 C_{x,y}\right)\frac{\partial\left(f(\delta)u_b\right)}{\partial z} \quad (39)$$

When $\frac{\partial\left(f(\delta)u_b\right)}{\partial z} < 0$ $\quad \lambda_1 = 1;\ \lambda_2 = 0$

When $\frac{\partial\left(f(\delta)u_b\right)}{\partial z} \geq 0$ $\quad \lambda_1 = 0;\ \lambda_2 = 1$

For the TZFBR, the kinetic models of combustion and gasification of coke must be added to the model described above.

A balance of the gaseous species must also be made at the point of mixing or feeding the reactants (H = h_f).
In addition, contributions to the change of H_2 flow because the permeation through the Pd-Ag membrane must be included in the TZFBR+MB, as will be discussed below.

A summary of the flows and exchanges between the different gas and solid phases considered in the TZFBR simulation is presented in Figure 4.

3.4 Model of flow through membranes

Eq. 40 describes the flow of H_2 through the membrane.

$$J_{H_2} = \frac{Pe_{H_2}}{\delta} \left(P^n_{H_2,R} - P^n_{H_2,P}\right) \quad (40)$$

Where J_{H2} represents the hydrogen flow, Pe_{H2} is the membrane permeability factor, δ is the thickness of the Pd layer, $P_{H2,R}$ is the partial pressure of H_2 in the retentate and $P_{H2,P}$ is the partial pressure of the H_2 in the permeate. The exponent n varies in the range of 0.5 - 1 and allows us to recognize the limiting step of permeation: if n = 0.5 (ideal case), Eq. 40 becomes the Sieverts - Fick law , diffusion is the limiting step; while, if n> 0.5 (deviations from Sieverts - Fick's law) the dissociation or recombination reactions are slower than diffusion or resistance to transport through the porous support affects the hydrogen flow. Temperature dependence is expressed as an Arrhenius law for permeability (Pe_{H2}), which can be substituted within Eq. 40 to obtain the so-called Richardson equation (Eq. 41)

$$J_{H_2} = J_0 \exp\left[-\frac{Ea_p}{RT}\right]\left(P^n_{H_2,ext} - P^n_{H_2,P}\right) \quad (41)$$

Where δ is considered within the constant J_0 and the pressure of H_2 in the retentate ($P_{H2,R}$) has been replaced by an average partial pressure of H_2 at the outer side of the membrane ($P_{H2,ext}$), which is considered a better approach.

To characterize the Pd-Ag membranes, permeation tests were performed using different H_2/Ar feed mixtures at different operating temperatures (500-525-550) ºC. An effect that is not usually taken into account when evaluating the membrane permeance, is the fact that the hydrogen partial pressure can change from the inlet to the outlet, so that the mean driving force is not necessarily the driving force calculated with partial pressure at the inlet or the outlet of the reactor. We have evaluated several possibilities to quantify the average driving force. Therefore, for the estimation of the average partial pressure of H_2 on the outer side of the membrane ($P_{H2,ext}$), the four approximations detailed by Montesinos et al. [44] where:

- $P_{H2,ext} \approx P_{H2,F}$
- $P_{H2,ext} \approx P_{H2,R}$

- $P_{H2,ext} \approx (P_{H2,F} + P_{H2,R})/2$
- $P_{H2,ext} \approx (P_{H2,F} - P_{H2,R})/ \log(P_{H2,F}/P_{H2,R})$

The parameters J_0 and E_{ap} were obtained by fitting the Richardson equation (Eq. 41) to the experimental permeation data, where the value of n is the one that optimizes the linear regression between the flow of H_2 and the driving force ($\Delta P_{H2} = P^n_{H2,ext} - P^n_{H2,P}$). The comparison of these possibilities shows that the use of a logarithmic mean driving force provides the best fit with n = 0.5.

Figure 5a shows the flow of H_2 through the membrane as a function of the driving force for different values of the coefficient n. The best fit is obtained when n = 0.5, which indicates that the permeation is controlled by diffusion and is close to being ideal. The dependence of permeation on temperature is presented in Figure 5b, which shows that the higher the temperature, the greater the permeation. By fitting the experimental results, the values for J_0 = 1.22 ($mL_{H2}/cm^2\ min\ mbar^{0.5}$) and E_{ap} = 13.33 (kJ mol^{-1}) were obtained.

For the simulation of TZFBR + MB it is necessary to have the H_2 permeation model, to this purpose the variation of the flow of H_2 because the permeation through the membrane has been expressed as a function of the reactor height, as follows:

$$\frac{dJ_{H_2}}{dz} = \frac{2r_m N_m}{r_R^2 - N_m r_m^2} J_0 \exp\left[-\frac{Ea_p}{RT}\right]\left(\sqrt{C_{H_2} RT} - \sqrt{P_{H_2,P}}\right) \quad (42)$$

3.5 Numerical methods

The mathematical models presented in section 3.3 correspond to partial differential equations (PDE) of hyperbolic type. The numerical solution of this type of models can be done by a well-established method for the solution of PDE, known as the method of lines (MOL), which has been applied to the main classes of PDE (parabolic, hyperbolic and elliptical) [45].

The basic idea of MOL is to replace the spatial derivatives of PDEs with algebraic approaches. This results in a system of ordinary differential equations (ODE) with an initial value variable that in our case is time. In this way, the original PDE is approached by a system of ODE.

The approximations in the spatial derivatives are made by finite differences, although there are other approximations that can be easily accommodated within the MOL format, for example, finite elements, finite volumes, etc.

The ODE system may be solved by applying any integration algorithm for initial value problems, thus providing an approximate numerical solution to the PDE.

Therefore, one of the most outstanding features of the MOL is the use of existing and generally well established numerical methods for the solution of ODE.

In the case of spatial integration, we can replace the derivative terms ($\partial C / \partial z$) in the balance equations with algebraic approximations, such as:

$$\frac{\partial C_i}{\partial z} \approx \frac{C_i - C_{i-1}}{\Delta z} \quad (43)$$

Where *i* is an index that represents the position along the mesh in z and Δz is the space between the points of the mesh. When *i* = 1, z = 0; *i* = n, z = H, where n is the number of mesh points and H is the height of the reactor bed.

In this work we have used the algorithms *dss004* (finite fourth order differences) and *dss012* (first order upwind) proposed by Schiesser [46] for the algebraic approximations of spatial derivatives. The *dss004* algorithm was used in the integration of the CFBR models while, due to the discontinuities in the flow of the species, in the TZFBR and TZFBR + MB the *dss012* algorithm gave better results. The MatLab® code of the two algorithms is available in literature.

For the integration of the temporal derivative ($\partial C / \partial t$) we can use the explicit methods of Euler or Runge Kutta. However, for stiff-type models these methods have stability problems related to the passage of time (Δt). Therefore, it is necessary to use implicit methods to calculate the temporary derivative. The advantages of using these methods lie in having better calculation stability and a decrease in simulation time. The methods that use the backward difference formula (BDF) are an alternative for solving stiff problems, although we will not go into detail with these methods.

MatLab® library has the *ode15s* integration algorithm that is based on BDF methods. This algorithm was used for the integration of the temporary derivative in this work.

To optimize the computing time, the dispersion pattern of the Jacobian matrix was calculated, which can be entered as an input argument in the *ode15s* function. This pattern allows optimizing the number of calls to the integration function and therefore the calculation time.

4. Model Validation

The results predicted by the mathematical model have been compared with the experimental results obtained in each of the three types of reactors: conventional fluidized bed reactor (CFBR), two-zone fluidized bed reactor (TZFBR) and two-zone fluidized bed reactor with membranes (TZFBR+MB).

4.1 Conventional FBR

The results obtained in the experiments carried out in CFBR at different reaction temperatures are shown in Figure 6. Due to the endothermic nature of the DRM

process, increasing the reaction temperature caused an increase in the initial conversion of CH_4 and in the yield and selectivity to H_2. The H_2/CO molar ratio also increased, since the DRM reaction (r.1) is more endothermic than the RWGS reaction (r.2).

The improvement in the conversion of CH_4 with temperature is due, firstly to the reaction kinetics (since the kinetic constants vary according to the Arrhenius equation), and secondly to the thermodynamic equilibrium (being an endothermic reaction). At 475°C an initial conversion value of about 20% was obtained, while conversions above 35% were obtained at 550°C.

Coke formation caused catalyst deactivation (Figure 6a), especially in the first 20 minutes of reaction, where a rapid drop in conversion values was noted. After 100 minutes of reaction, catalyst deactivation was slower, which would indicate that the coke formation rate had decreased. As seen in the kinetic study, coke formation tends to balance with its gasification, gradually reducing the catalyst deactivation rate.

Like the conversion, both the yield (Figure 6b) and the selectivity to H_2 (Figure 6c) increased with temperature. In the range studied, yields varying from 10% to 25% and selectivities from 55% to 70% were obtained. The yield decreased slightly as the reaction time progressed, due to the catalyst deactivation, while the selectivity changed in the opposite way, slightly increasing. The increase in selectivity to hydrogen when the conversion decreases can be explaining by considering that, from the point of view of hydrogen production, dry reforming of methane (r.1) and the reverse water-gas-shift (r.2) are reactions in series. In any set of series reactions, the selectivity to the intermediate product is higher for smaller conversion.

Figure 6d shows the variation of the H_2/CO molar ratio as a function of CH_4 conversion for different reaction temperatures. For all the temperatures studied, initial H_2/CO values close to 1 were obtained, while for the final reaction time (240 min), it depends on temperature, having values between 0.75 and 0.82 for the temperature range studied.

Figure 6 also shows the predictions of the model, which were very satisfactory, since they follow the same trends as the experimental data.

4.1.2 Effect of space time

Experimental tests were performed with different spatial times (W/F_{CH4o}). For this purpose, we worked with different catalyst weights (1, 5 and 30 g) and the feed rate was kept constant. In order to keep the catalytic bed height constant and therefore the dynamics of the fluidized bed, the catalyst was mixed with inert alumina with the same particle size distribution (106-180 μm).

Figure 7 shows the results obtained in the experiments performed at different spatial times. For small values, an initial conversion of CH_4 (Figure 7a) close to 20% was obtained and initial yields to H_2 (Figure 7b) were around 15%. However, these values declined dramatically at higher time-on-stream due to catalyst deactivation by coke. At high space time the catalyst deactivation is less noticeable, i.e. the change in conversion along time-on-stream is slower. This is a common result in any catalytic reactor operating in integral way, particularly when the initial yield is close to the thermodynamic limit because the high space time. Conversions and yields around 25% and 18% respectively were obtained, while the selectivity to H_2 was over 70% (Figure 7c).

As for the H_2/CO molar ratio (Figure 7d), its value increased as space time was increased. Values of 0.6 were obtained with small space times while for larger space times, H_2/CO molar ratios greater than 0.8 were obtained.

The model predictions satisfactorily follow well the trends of the experimental data.

4.1.3 Effect of feed composition

Figure 8 shows the results obtained in the experiments performed with different feed compositions. The feed with excess CO_2 respect to the stoichiometric ratio gave an initial conversion of CH_4 (Figure 8a) about 35% and an initial yield to H_2 (Figure 8b) of 20%, while for the feed with excess CH_4 an initial conversion of CH_4 of 25% and an initial yield of H_2 close to 18% were achieved. Considering only the conversion and yield values, favorable conditions would be met when working with excess CO_2 in the feed. However, the H_2/CO molar ratio (Figure 8d) was affected by the feed composition, having values of 0.7 for feed with excess CO_2 and values greater than 1 for feed with excess CH_4. It is also true that an excess of CO_2 in the feed compared to the stoichiometric one implied a lower concentration of H_2 in the obtained stream, although methane conversion was greater.

Therefore, if a process with high conversion and performance is required, it would be necessary to operate with feeds with excess CO_2; in the same way, if a process with high selectivity to H_2 and a molar ratio value H_2/CO greater than 1 is required, it should be operated with excess CH_4. The feed percentages of the reactant gases can be varied so that a desired value of the H_2/CO molar ratio would be obtained.

In these experiments the catalyst deactivation by coke formation is also noted, especially in the initial minutes of the reaction.

As for the simulation, the data predicted by the models follow the trends of the experimental data, verifying that the proposed model is well suited to respond to the different operating conditions tested in this work.

4.2 Two zone fluidized bed reactor (TZFBR)

The experimental data of DRM process carried out in the TZFBR configuration were obtained in previous works performed in our group [26,27], using the experimental system described in section 2. The operating conditions of these experiments are presented in Table 2.

Table 2. Experimental operating conditions for DRM in TZFBR

Exp	T	O_x	$CH_4\|CO_2\|N_2\|O_x$	CFBR	TZFBR	h_f
				stage 1	*stage 2*	
	(°C)		(%)	(min)	(min)	(cm)
1	500	CO_2	30|30|32|8,0	10	187	2.0
2	525	CO_2	30|30|32|8,0	120	150	2.0
3	525	O_2	30|30|36,5|3,5	10	150	2.0
4	525	CO_2	30|30|32,0|8,0	10	150	2.0

The effects of the reaction temperature and the percentage and nature of the regenerating gas (Ox), either O_2 or CO_2, were evaluated. All experiments presented in Table 2 were performed with a total feed rate of 235.5 mL(STP).min^{-1}, a relative gas velocity (u_r) of 3 and a catalyst weight (W) of 30 g. In addition, each experiment was carried out in two stages: stage 1, which corresponds to the time in which the reactor was operated under the CFBR conditions, this being necessary for the process to reach reaction stability and stage 2, when regenerating gas (Ox) was introduced through the bottom of the reactor, thus forming the conditions of the TZFBR configuration.

4.2.1 Effect of temperature

The results obtained for experiments 1 and 2 when working in TZFBR configuration (i.e. stage 2), each performed at a different temperature, are presented in Figure 9. As in CFBR, increases in CH_4 conversion, yield to H_2, selectivity to H_2 and the H_2/CO molar ratio were seen with the increase in temperature.

In both experiments, the loss of catalyst activity due to coke formation can be seen, being more noticeable in experiment 1 carried out at 500 ° C. The difference between the two experiments lies in the initial reaction stage (stage 1, not shown in the figure), where it was operated under the CFBR conditions, in one case 10 minutes (experiment 1) and in the other case 120 minutes (experiment 2). As already mentioned above, the greatest deactivation of the catalyst occurs in the first minutes of reaction, therefore, in experiment 2, where stage 1 has a duration of 120 minutes, deactivation of the

catalyst in stage 2 (TZFBR) is less noticeable, because the catalyst is regenerated in the lower zone of the reactor, which causes the loss of catalytic activity to be slower. In both cases the percentage of regenerating gas (8% CO_2) fed to the reactor was insufficient to achieve stability in the process.

Simulation data were obtained, in the same way, by stages, where the data obtained at the end of one stage serve as initial conditions for the next stage. It can be seen (Figure 9) that the data predicted by the models follow the same trend as the experimental data. This is important, since it validates the proposed kinetic models for the main reaction, for the catalyst deactivation and for the coke combustion/ gasification reactions, which are used within the mathematical model of the TZFBR.

4.2.2 Effect of the amount and nature of the regenerating gas

Figure 10 presents the results obtained in the experiments performed with different regenerating gases. While O_2 is the most commonly used gas to regenerate deactivated catalysts, CO_2 can also be an alternative regenerating agent to gasify coke.

In the TZFBR configuration, catalyst regeneration was studied by combustion (with O_2) and gasification (with CO_2) of coke (experiments 3 and 4, Table 2). For the combustion, a diluted stream of O_2 (3.5% of the total feed flow) was used, while for gasification, a dilute stream of CO_2 with 8% of the total flow was used. The experiments were carried out in two stages: stage 1 operating under CFBR conditions, with a duration of 10 min and stage 2 where it was operated under TZFBR conditions. The graphs presented correspond only to the data obtained in stage 2.

The initial values of conversion, yield and selectivity were similar to the values obtained in the CFBR configuration at 525°C, however, as the reaction time progressed the TZFBR configuration experienced less deactivation, thanks to the catalyst regeneration in the lower zone of the reactor.

Regarding the H_2/CO molar ratio (Figure 10d), when CO_2 was used as a regenerating gas, CO was generated in the lower zone of the reactor, which passed into the reaction zone, generating a decrease in the H_2/CO molar ratio. The amount of CO formed by coke gasification (reverse of r.4) from a feed with 8% of CO_2 is larger than from a feed with 3.5% of O_2.

The data predicted by the models present the same trends as the experimental data for the two cases of regeneration (O_2/CO_2). The TZFBR configuration also exhibited some catalyst deactivation in these experiments due to coke formation, but the trend is towards a steady state after a few hours. Probably, in order to quickly achieve a fully stable process, the percentage of regenerating gas fed to the reactor could be increased.

4.2.3 Coke formation

Since experimental data on coke concentration versus time are not available, Figure 11 shows only the coke concentration data predicted by the models. In the TZFBR configuration the evolution of the coke concentration with the reaction time depends on factors such as reaction temperature and percentage and nature of the regenerating gas. At a lower reaction temperature, coke formation side reactions are favored; therefore, the experiment carried out at 500°C has a higher coke concentration. As for the regenerating gas, both O_2 and CO_2 have proven to be effective agents in recovering the catalyst activity. However, the percentages used in the feed were not sufficient to achieve a stable behavior and, therefore, a higher percentage of regenerating agent will be necessary to achieve a balance between the formation and consumption of coke. It must be taken into account that in the coke gasification, and due to the different stoichiometry of reactions between coke and CO_2 or O_2, a higher percentage of CO_2 in the feed will be needed to match the results obtained with O_2.

4.3 Two-zone fluidized bed reactor with membranes (TZFBR+MB)

Like the previous configuration (TZFBR), the experimental data of the DRM process in the TZFBR+MB configuration were previously obtained [26,27], in the experimental system described in section 2. The operating conditions of these experiments are presented in Table 3.

Table 3. Experimental operating conditions for DRM in TZFBR+MB.

Exp	**T** (°C)	**O_x**	**CH_4|CO_2| N_2|O_x** (%)	**CFBR** *stage 1* (min)	**TZFBR+MB** *stage 2* (min)	**h_f** (cm)
1|2	475	O_2	30|30|30|10	120	360	2|4.5
3|4	500					
5|6	525					
7|8	550					
9|10	575					
11|12	550		30|30|35|5.0			
13|14			30|30|32.5|7.5			
15|16		CO_2	30|30|10|30			
17		O_2	30|30|35|5.0	0	480	4.5
18			30|30|32.5|7.5			
19			30|30|30|10			

In these experiments, the effect of temperature, the percentage and nature of the regenerating gas, the height of the regeneration zone and the time or period of activation of the membranes were evaluated. All experiments presented in Table 3 were performed with a total feed rate of 235.5 mL(STP) .min^{-1}, a relative gas velocity

(u_r) of 3 and a catalyst weight of 30 g. Mixtures of catalyst with inert alumina (with the same size distribution) were made to reach a height of 30 cm catalytic bed. This allowed the membranes to be completely submerged within the reaction zone, while the height of the regeneration zone could be varied (h_f = 2 cm, h_f = 4.5 cm) by changing the position of the rod through reactants were fed.

Experiments 1 to 16 were carried out in two stages: stage 1 corresponds to the time in which it is operated under the CFBR conditions, this being necessary for the process to reach reaction stability and also the membranes comply with an activation period, which prevents rapid loss of catalyst activity at the start of the reaction as set forth by Ugarte et al. [26], and step 2, in which regenerating gas was introduced through the bottom of the reactor and the operation of the membranes that selectively extract hydrogen was activated, thus forming the conditions TZFBR + MB. Experiments 17 to 19 operate under the TZFBR + MB conditions without the activation period.

4.3.1 Effect of temperature and height of the regeneration zone (h_f)

Figure 12 shows the results obtained at different operating temperatures. Both the CH_4 conversion and the H_2 yield reached their best results as the temperature increases. On the other hand, the selectivity to H_2 varies very little with the temperature and, finally, the H_2/CO molar ratio decreases with the increase in temperature.

At low reaction temperature (475°C), an increase in CH_4 conversion was observed with the reaction time and a H_2/CO molar ratio greater than 2, which also increases with the reaction time. This is due to the effect caused by the membranes, which extract H_2 selectively, promoting the reactions that form H_2. That is, at low temperatures and in addition from the main reaction (DRM-r1) other reactions of hydrogen formation (Methane decomposition -r.4) and coke consumption (Coke gasification by H_2O-r5) are also promoted. Therefore, the coke from stage 1 was consumed in the regeneration zone by the regenerating gas and also in the reaction zone by gasification with water vapor, thus recovering much of the catalyst activity. At slightly higher temperatures (525°C), the use of membranes promoted the reaction of methane decomposition (r.4), but no longer the reaction of coke gasification with water vapor (r.5). This fact explains why the catalyst deactivated by increased coke formation. For high operating temperatures (550 - 575°C) the process is close to the balance between the formation and consumption of coke, with little catalyst deactivation.

The data obtained in the simulation predict the experimental trends quite well, showing the same variation with the temperature and the same stability with the reaction time.

A similar effect was observed with the experiments performed with h_f = 4.5 cm (not shown). In addition to gaining stability in the process, slightly lower values of CH_4 conversion and H_2 yield were obtained. This is due to the slightly higher dilution of the catalyst particles in the bed with inert alumina particles. Therefore, although the height of the reaction zone was the same, its catalyst content was slightly lower, which led to a small drop in conversion.

4.3.2 Effect of the amount and nature of the regenerating gas

In order to reduce the catalyst deactivation by coke formation, the percentage and nature of the regenerating gas was changed. Therefore, experiments were performed using O_2 (5%, 7.5% and 10%) and also CO_2 (30%) as catalyst regenerating agents. The conditions of these experiments (11 to 16) are shown in Table 3. The percentage of the regenerating gas is calculated with reference to the total feed flow.

Figure 13 shows the results obtained (X_{CH4}, Y_{H2}, S_{H2} and H_2/CO) for this series of experiments, with a height of the regeneration zone of 4.5 cm (h_f). In general terms, the improvement in H_2 yield with the TZFBR + MB configuration was similar, regardless of the amount and nature of the regenerating gas used. Therefore, an average H_2 yield of 55% was obtained versus the 25% obtained in the CFBR configuration at the same reaction temperature (550°C).

Regarding the stability of the process, when O_2 was used as a regenerating gas and a height of the regeneration zone (h_f) of 4.5 cm, the higher the percentage of O_2 fed, the more stable the process. With 5% O_2 the mean rate of change in conversion was 0.67 percentage points per hour, and it decreased to only 0.04 percentage points per hour with 10% O2 in the feed. Regarding the use of CO_2 as a regenerating gas, it was necessary to work with a high percentage (30% of CO_2) in the feed and a large regeneration zone (h_f = 4.5 cm) to achieve results close to those obtained with O_2. Due to the slower reaction kinetics with CO_2 as an oxidant, more height of the regeneration zone and/or a larger percentage of the CO_2 in the feed were required to reach steady state conditions. In that case, the rate of change in conversion was 0.9 percentage points per hour, even higher than that achieved with only 5% O_2.

Therefore, it is determined that CO_2 can be used as a catalyst regenerating agent for the DRM process and that an adequate amount of CO_2 provides stability similar to when O_2 is used as a regenerant. In addition, in some cases, CO_2 may be preferable from the point of view of process safety. Two additional considerations must be taken into account when working with the TZFBR+MB configuration using O_2 as regenerating agent. On the one hand, a high percentage of O_2 in the current fed to the regeneration zone favors the elimination of coke and, consequently, the stability of the process. On

the other hand, if there is an excess of O_2, it could reach the reaction zone. Then, in addition to producing unwanted oxidation of some part of CH_4, CO or H_2, this O_2 could oxidize the active metal phase of the catalyst (Ni and Ce) and gradually deactivate it [47, 48].

4.3.3 Effect of the initial activation period

To avoid an oxidizing atmosphere in which the metal oxidizes and, consequently, decreases its activity [49], we initially considered suitable to start the process without hydrogen extraction for a period of time before activating the functioning of the membranes. In this way, an activation stage was implemented (stage 1) in which the system worked under the CFBR conditions without hydrogen extraction [26]. The effect of eliminating this preliminary stage was analyzed with a series of experiments (17 to 19), performed with different percentages of O_2 as a regenerating gas and a height of the regeneration zone (h_f) of 4.5 cm (Table 5.3).

Figure 14 presents the results of experiments performed without the activation stage of the membranes. These results show no differences by eliminating said activation stage, since the conversion values, yield, selectivity and molar ratio H_2/CO were quite similar to those obtained with the activation stage. This implies that the process can be started under conditions of the TZFBR+MB configuration, without being penalized in terms of activity or stability. With 5% O_2 the mean rate of change in conversion was 0.94 percentage points per hour, and it decreased to 0.51 and 0.43 percentage points per hour with 7.5 and 10% O_2 in the feed, respectively.

4.3.4 Coke formation

Figure 15 shows the coke concentration data as a function of time obtained by simulation at different operating conditions for stage 1 and 2. Coke concentrations decrease in stage 1 as the reaction temperature increases, as observed in the results obtained with the CFBR configuration, in addition these results are consistent with the trend indicated by thermodynamic equilibrium.

In stage 2 the effect of the membranes is observed. As discussed above, at 475°C in the TZFBR with the presence of membranes, coke gasification is promoted. Above 500°C coke formation decreases as the reaction temperature increases, having the lowest coke concentration at 575°C.

The percentage and nature of the regenerating gas also determines the amount of coke present at the end of the reaction. Thus, the experiments performed with 10% O_2 in the regeneration stream presented coke concentrations around 0.07 (g_{coke} / g_{cat})

after 8 hours of reaction at 550°C, while the experiments performed with 30% of CO_2 presented coke concentrations near 0.1 (g_{coke} / g_{cat}).

The activation stage of the membranes has no major influence on the formation of coke, since the simulation scenarios proposed with and without this stage have similar coke concentrations at the end of the reaction. In the experiment performed without the activation stage (stage 1) it can be seen that the membranes promote coke formation, i.e. the achieved coke concentration was higher than without membranes, at the same reaction temperature. This can be explained by increased decomposition of CH_4 (reaction r.3) when removing H_2.

It is also worth mentioning that by increasing the height of the regeneration, the final coke concentration decreased, this decrease being more relevant in the regeneration with CO_2 than with O_2. This difference between CO_2 and O_2 can be explained by the fact that the regeneration reaction with oxygen occurs almost entirely in the first centimeters of the regeneration zone, therefore, a point will come at which increasing the height of the regeneration zone would no longer have any effect. On the contrary, the reaction with CO_2 is slower than with O_2, and the increase of the height of the regeneration zone allows higher CO_2 conversion in this zone.

5. Conclusion

A mathematical model based on three-phase model of fluidized bed reactors and the kinetic equations previously developed can describe the performance of several innovative reactors for dry reforming of methane: a) Conventional Fluidized Bed Reactor, b) Two-Zone Fluidized Bed Reactor, c) Two-Zone Fluidized Bed Reactor with Membranes.

The model describes well the conversion of methane, hydrogen yield, selectivity to hydrogen and H_2/CO ratio obtained in the three reactor configurations, including the evolution with time-on-stream. The model also describes well the effect of several operation variables, such as the amount of regenerating gas, the effect of using O_2 or CO_2 as regenerating gas, the operation temperature or the spatial time.

The model predicts well the improvement in stability obtained when changing the conventional fluidized bed reactor to the two-zone fluidized bed reactor, thanks to the in-situ regeneration achieved in the lower zone of the later. It also predicts the improvements in yield that can be achieved by the use of a two-zone fluidized bed reactor with membranes.

Finally, the model allows evaluating the evolution along time of coke concentration in each reactor configuration, a result that would be very difficult to obtain experimentally. This helps to understand how the catalyst deactivation by coke and the catalyst regeneration are affecting the reactor performance.

The validity of this mathematical model would make it a useful tool to optimize the reactor performance and to explore the best configuration if this kind of reactor is scaled-up or included in an industrial process.

Acknowledgements

Financial support from the Spanish Ministerio de Economía e Innovación (MINECO) through the project CTQ2016-76533-R is gratefully acknowledged.

Nomenclature

Variable	Description	Units
$C_{i,b}$	Concentration of *i* compound in bubble (b) and emulsion (e) phase	[mol cm^{-3}]
$C_{i,e}$		
C_c	Coke concentration	[g g_{cat}^{-1}]
d_b	Bubble diameter	[cm]
d_{bm}	Maximum bubble diameter	[cm]
D_i	Internal reactor diameter	[cm]
D_{im}	Diffusion coefficient in a mixture of gases	[cm^2 s^{-1}]
d_{orif}	Diameter of the orifice of the feed entry located at height h_f	[cm]
E_{ap}	Activation energy for hydrogen permeation	[kJ mol^{-1}]
ε_{mf}	Minimum fluidization porosity	[-]
f_w	Fraction of bubble volume occupied by the wake	[-]
H	Total bed height	[cm]
h_f	Height of the intermediate feed entry	[cm]
J_{H2}	Flow of hydrogen through the membrane	[mol m^{-2} s^{-1}]
J_o	Preexponential factor for hydrogen flux	[mol m^{-1} s^{-1} $Pa^{-0.5}$]
K_{be}	Gas Exchange coefficient between bubble and emulsion and viceversa	[s^{-1}]
K_{eb}		
K_{ew}	Solid Exchange coefficient between wake and emulsion and viceversa	[cm^{-1}]
K_{we}		

N_m	Number of membranes	[-]
r	Reaction rate	[mol g_{cat} s^{-1}]
r_m	Radius of the membrane	[cm]
r_R	Radius of the reactor	[cm]
u_b	Bubble rise rate	[cm s^{-1}]
u_e	Gas velocity in emulsion	[cm s^{-1}]
u_{mf}	Minimum fluidization velocity	[cm s^{-1}]
u_s	Downward velocity of solid in emulsion	[cm s^{-1}]
u_{sg}	Gas velocity	[cm s^{-1}]
$u_{sg,1}$	Gas velocity in the regeneration zone	[cm s^{-1}]
$u_{sg,2}$	Gas velocity in the reaction zone	[cm s^{-1}]
W	Weigth of catalyst	[g]
δ	Volume fraction of bed in bubbles	[-]
subscrips		
b	Bubble	
e	Emulsion	
i	Gas species	
j	Solid species (coke)	
w	Wake	

References

[1] D. Zambrano, J. Soler, J. Herguido, M. Menéndez, Kinetic Study of Dry Reforming of Methane Over Ni–Ce/Al_2O_3 Catalyst with Deactivation, Top. Catal. 62 (2019) 456–466.

[2] F. Fischer and H. Tropsch , The composition of products obtained by the petroleum síntesis, Brennst Chemistry 39 (3) (1928)

[3] T. Degnan, Low Temperature plasma reforming of CH_4-CO_2 with catalysts-a one step process to liquid oxygenates, Focus on Catal., Nov. 2017, page 1

[4] J.R.H. Ross, Natural gas reforming and CO_2 mitigation, Catal. Today. 100 (2005) 151–158.

[5] B. Fidalgo, J.Á. Menéndez, Carbon materials as catalysts for decomposition and CO_2 reforming of methane: A review, Chinese J. Catal. 32 (2011) 207-216.

[6] D. Pakhare, J. Spivey, A review of dry (CO_2) reforming of methane over noble metal catalysts, Chem. Soc. Rev. 43 (2014) 7813-7873.

[7] J.-M. Lavoie, Review on dry reforming of methane, a potentially more environmentally-friendly approach to the increasing natural gas exploitation., Front. Chem. 2 (2014) art 81.

[8] M. Usman, W.M.A. Wan Daud, H.F. Abbas, Dry reforming of methane: Influence of process parameters—A review, Renew. Sustain. Energy Rev. 45 (2015) 710–744.

[9] P. Prasad, S.S.E.H. Elnashaie, Novel circulating fluidized-bed membrane reformer for the efficient production of ultraclean fuels from hydrocarbons, Ind. Eng. Chem. Res. 41 (2002) 6518-6527.

[10] J. Herguido, M. Menéndez, J. Santamaría, On the use of fluidized bed catalytic reactors where reduction and oxidation zones are present simultaneously, Catal. Today. 100 (2005) 181–189.

[11] J. Herguido, M. Menéndez, Advances and trends in two-zone fluidized-bed reactors, Curr. Opin. Chem. Eng. 17 (2017) 15-21.

[12] J. Soler, J. M. López Nieto, J. Herguido, M. Menéndez, J. Santamaría, Oxidative Dehydrogenation of n-Butane in a Two-Zone Fluidized-Bed Reactor, Ind. Eng. Chem. Res.,38 (1999) 90-97.

[13] M.L. Pacheco, J. Soler, A. Dejoz, J.M. López Nieto, J. Herguido, M. Menéndez, J. Santamaría, MoO3/MgO as a catalyst in the oxidative dehydrogenation of n-butane in a two-zone fluidized bed reactor, Catal. Today 61 (2000) 101–107

[14] O. Rubio, J. Herguido, M. Menéndez, Two-zone fluidized bed reactor for simultaneous reaction and catalyst reoxidation: influence of reactor size, Applied Catal. A: Gen. 272 (2004) 321–327.

[15] J. Gascón, C. Téllez, J. Herguido, M. Menéndez, Fluidized bed reactors with two-zones for maleic anhydride production: Different configurations and effect of scale, Ind. Eng. Chem. Res. 44 (2005) 8945–8951.

[16] A.M. Adris, S. Elnashaie, R. Hughes, A fluidized-bed membrane reactor for the steam reforming of methane, Can. J. Chem. Eng. 69 (1991) 1061-1070.

[17] A.M. Adris, C.J. Lim, J.R. Grace, The fluidized-bed membrane reactor for steam methane reforming: model verification and parametric study, Chem. Eng. Sci. 52 (1997) 1609-1622.

[18] A. Mahecha-Botero, T. Boyd, A. Gulamhusein, N. Comyn, C.J. Lim, J.R. Grace, Y. Shirasaki, I. Yasuda, Pure hydrogen generation in a fluidized-bed membrane reactor: Experimental findings, Chem. Eng. Sci. 63 (2008) 2752–2762.

[19] Z. Chen, J. Grace, C. J. Lim, A. Li, Experimental studies of pure hydrogen production in a commercialized fluidized-bed membrane reactor with SMR and ATR catalysts, Int. J. Hydrog. Energy. 32 (2007) 2359–2366.

[20] A. Mahecha-Botero, J.R. Grace, C. Jim Lim, S.S.E.H. Elnashaie, T. Boyd, A. Gulamhusein, Pure hydrogen generation in a fluidized bed membrane reactor: Application of the generalized comprehensive reactor model, Chem. Eng. Sci. 64 (2009) 3826–3846.

[21] F. Gallucci, M. van Sint Annaland, J.A.M. Kuipers. Theoretical comparison of packed bed and fluidized bed membrane reactors for methane reforming. Int. J. Hydrogen Energy, 35 (2010) 7142-7150.

[22] A. Helmi, E. Fernandez, J. Melendez, D.A.Pacheco Tanaka, F. Gallucci, M. Van Sint Annaland, Fluidized bed membrane reactors for ultra pure H_2 production - A step forward towards commercialization, Molecules. 21 (2016).

[23] A. Arratibel, J.A. Medrano, J. Melendez, D.A. Pacheco Tanaka, M. van sint Annaland, F. Gallucci, Attrition-resistant membranes for fluidized-bed membrane reactors: Double-skin membranes, J. Membr. Sci.,563 (2018) 419-426.

[24] M.P. Gimeno, Z.T. Wu, J. Soler, J. Herguido, K. Li, M. Menéndez, Combination of a two-zone fluidized bed reactor with a Pd hollow fibre membrane for catalytic alkane dehydrogenation. Chem. Eng. J.,155 (2009) 298-303.

[25] J.A. Medrano, I. Julián, F.R. García-García, K. Li, J. Herguido, M. Menéndez. Two-zone fluidized bed reactor (TZFBR) with palladium membrane for catalytic propane

dehydrogenation: experimental performance assessment. Ind. Eng. Chem. Res.,52 (2013) 3723-3731.

[26] P. Ugarte, P. Durán, J. Lasobras, J. Soler, M. Menéndez, J. Herguido. Dry reforming of biogas in fluidized bed: process intensification. Int. J. Hydrog. Energy, 42 (2017) 13589-13597.

[27] P. Durán, A. Sanz-Martínez, J. Soler, M. Menéndez, J. Herguido, Pure hydrogen from biogas: Intensified methane dry reforming in a two-zone fluidized bed reactor using permselective membranes, Chem. Eng. J. 370 (2019) 772–781.

[28] K. Hou, M. Fowles, R. Hughes, Potential catalyst deactivation due to hydrogen removal in a membrane reactor used for methane steam reforming, Chem. Eng. Sci. 54 (1999) 3783–3791.

[29] M.N. Pedernera, J. Piña, D.O. Borio, Kinetic evaluation of carbon formation in a membrane reactor for methane reforming, Chem.Eng. J. 134 (2007) 138–144.

[30] R. Schafer, M.Noack, P.Kolsch, M. Stohr, J. Caro, Comparison of different catalysts in the membrane-supported dehydrogenation of propane, Catalysis Today 82 (2003) 15–23.

[31] J. Soler, C. Tellez, J. Herguido, M. Menéndez, J. Santamaría, Modelling of a two-zone fluidised bed reactor for the oxidative dehydrogenation of n -butane, Powder Technol. 120 (2001) 88–96

[32] O. Rubio, J. Herguido, M. Menéndez, G. Grasa, J.C. Abanades, Oxidative Dehydrogenation of Butane in an Interconnected Fluidized-Bed Reactor, AIChE J. 50 (2004) 1510-1522.

[33] J. Gascón, C. Téllez, J. Herguido, H.A. Jakobsen, M. Menéndez, Modeling of fluidized bed reactors with two reaction zones, AIChE J. 52 (2006) 3911–3923.

[34] D. Kunii, O. Levenspiel, Fluidization engineering, Butterworth-Heinemann, 1991.

[35] J.F. Davidson, D. Harrison, The behavior of a continuously bubbling fluidized bed, Chem. Eng. Sci. 21 (1966) 731–738.

[36] S. Mori, C.Y. Wen, Estimation of bubble diameter in gaseous fluidized beds, AIChE J. 21 (1975) 109–115.

[37] D. Kunii, O. Levenspiel, Bubbling bed model: Model for the Flow of Gas through a Fluidized Bed, Ind. Eng. Chem. Fundam. 7 (1968) 446–452.

[38] I. Julián, J. Herguido, M. Menéndez, A non-parametric bubble size correlation for a Two-Section Two-Zone Fluidized Bed Reactor (TS-TZFBR), Powder Technol. 256 (2014) 146–157.

[39] D. Kunii, O. Levenspiel, Bubbling bed model for kinetic processes in fluidized beds: Gas-Solid Mass and Heat Transfer and Catalytic Reactions, Ind. Eng. Chem. Process Des. Dev. 7 (1968) 481–492.

[40] Z. Zhou, L. Han, G.M. Bollas, Model-assisted analysis of fluidized bed chemical-looping reactors, Chem. Eng. Sci. 134 (2015) 619–631.

[41] S. Sane, H. Haynes, P.K. Agarwal, An experimental and modelling investigation of gas mixing in bubbling fluidized beds, Chem. Eng. Sci. 51 (1995) 1133–1147.

[42] S. Sriramulu, S. Sane, P. Agarwal, T. Mathews, Mathematical modelling of fluidized bed combustion: 1. Combustion of carbon in bubbling beds, Fuel. 75 (1996) 1351–1362.

[43] R.A. Srinivasan, S. Sriramulu, S. Kulasekaran, P.K. Agarwal, Mathematical modeling of fluidized bed combustion — 2: combustion of gases, Fuel. 77 (1998) 1033–1049.

[44] H. Montesinos, I. Julián, J. Herguido, M. Menéndez, Effect of the presence of light hydrocarbon mixtures on hydrogen permeance through Pd - Ag alloyed membranes, Int. J. Hydrog. Energy 40 (2014) 3402-3471.

[45] W.E. Schiesser, G.W. Griffiths, A Compendium of Partial Differential Equation Models : Method of Lines Analysis with Matlab, 2009.

[46] W.E. Schiesser, Partial Differential Equation Analysis in Biomedical Engineering case studies with Matlab, 2013.

[47] C. Wang, N. Sun, N. Zhao, W. Wei, Y. Sun, C. Sun, H. Liu, C.E. Snape, Coking and deactivation of a mesoporous Ni-CaO-ZrO_2 catalyst in dry reforming of methane: A study under different feeding compositions, Fuel. 143 (2015) 527–535.

[48] Z. Hou, J. Gao, J. Guo, D. Liang, H. Lou, X. Zheng, Deactivation of Ni catalysts during methane autothermal reforming with CO_2 and O_2 in a fluidized-bed reactor, J. Catal. 250 (2007) 331–341.

[49] P. Djinović, I.G.O. Črnivec, A. Pintar, Biogas to syngas conversion without carbonaceous deposits via the dry reforming reaction using transition metal catalysts, Catal. Today. 253 (2015) 155–162.

Figure captions

Figure 1. Scheme of the three configurations: a) Conventional Fluidized Bed Reactor (CFBR), b) Two-Zone Fluidized Bed Reactor (TZFBR), c) Two-Zone Fluidized Bed Reactor with membranes (TZFBR+MB)

Figure 2. Three-phases model for Fluidized bed reactors

Figure 3. Scheme representing the terms of the mass balances for gases and solid.

Figure 4. Scheme of the flow model considered for TZFBR/TZFBR+MB

Figure 5. (a) H_2 permeation flux at T = 500 °C for several values of *n*. (b) Effect of temperature on the H_2 permeation flux through a Pd-Ag membrane. In both cases $P_{H2,ext} \approx (P_{H2,F} - P_{H2,R})/\log(P_{H2,F}/P_{H2,R})$.

Figure 6. Effect of reaction temperature in CFBR. a) CH_4 conversion. (b) Yield of H_2. (c) Selectivity to H_2. (d) H_2/CO molar ratio. W = 30 g, u_r = 3, $CH_4|CO_2|N_2$ = 40|40|20, time-on-stream = 240 min. Experimental data (symbols), model prediction (lines).

Figure 7. Effect of spatial time in CFBR. (a) CH_4 conversion. (b) Yield of H_2. (c) Selectivity to H_2. (d) H_2/CO molar ratio. T = 525 ºC, u_r = 3, $CH_4|CO_2|N_2$ = 40|40|20, time on stream = 240 min. Experimental data (symbols), model prediction (lines).

Figure 8. Effect of feed composition. (a) CH_4 conversion. (b) Yield of H_2. (c) Selectivity to H_2. (d) H_2/CO molar ratio. T = 525 ºC, u_r = 3, $CH_4|CO_2|N_2$ = 40|40|20, time on stream = 240 min. Experimental data (symbols), model prediction (lines).

Figure 9. Effect of reaction temperature in a TZFBR. (a) CH_4 conversion. (b) Yield of H_2. (c) Selectivity to H_2. (d) H_2/CO molar ratio. W = 30 g, u_r = 3. Ox = 8% CO_2.. Experimental data (symbols), model prediction (lines).

Figure 10. Effect of using O_2 or CO_2 as regenerating gas in a TZFBR. (a) CH_4 conversion. (b) Yield of H_2. (c) Selectivity to H_2. (d) H_2/CO molar ratio. T = 525 ºC. W = 30 g, u_r = 3. W = 30 g, u_r = 3. Ox = 8% CO_2. Experimental data (symbols), model prediction (lines).

Figure 11. Coke concentration along time-on-stream in a CFBR (stage 1=10 min), TZFBR (stage 2=200 min).

Figure 12. Effect of reaction temperature operating as TZFBR+MB. (a) CH_4 conversion. (b) Yield of H_2. (c) Selectivity to H_2. (d) H_2/CO molar ratio. W = 30 g, u_r = 3. h_f = 2 cm. Experimental data (symbols), model prediction (lines).

Figure 13. Effect of the amount and nature of regenerating gas in TZFBR+MB. (a) CH_4 conversion. (b) Yield of H_2. (c) Selectivity to H_2. (d) H_2/CO molar ratio. T = 550 °C. W = 30 g, u_r = 3. h_f = 4.5 cm. Experimental data (symbols), model prediction (lines).

Figure 14. Results when no activation stage (stage 1) was used in TZFBR+MB. (a) CH_4 conversion. (b) Yield of H_2. (c) Selectivity to H_2. (d) H_2/CO molar ratio. T = 550 °C. W = 30 g, u_r = 3. h_f = 4.5 cm Experimental data (symbols), model prediction (lines).

Figure 15. Coke concentration vs time-on-stream predicted by the mathematical model at different operating conditions: (a) temperatures, (b) h_f and amount and nature of regenerating gas in TZFBR configuration.

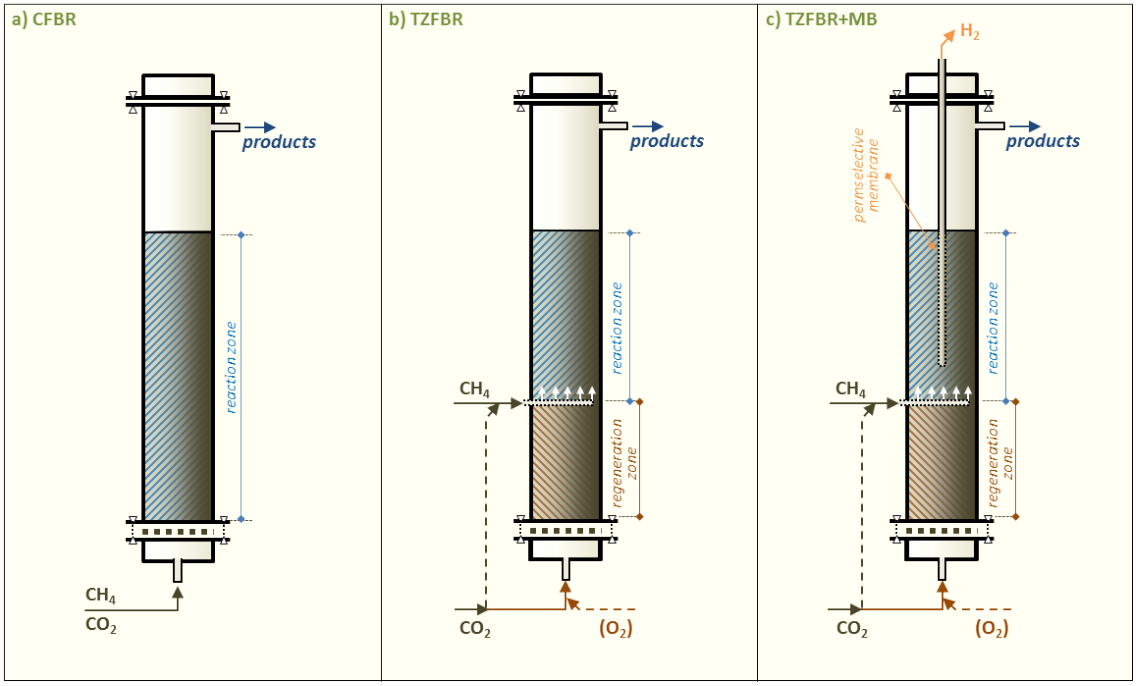

Figure 1. Scheme of the three configurations: a) Conventional Fluidized Bed Reactor (CFBR), b) Two-Zone Fluidized Bed Reactor (TZFBR), c) Two-Zone Fluidized Bed Reactor with membranes (TZFBR+MB)

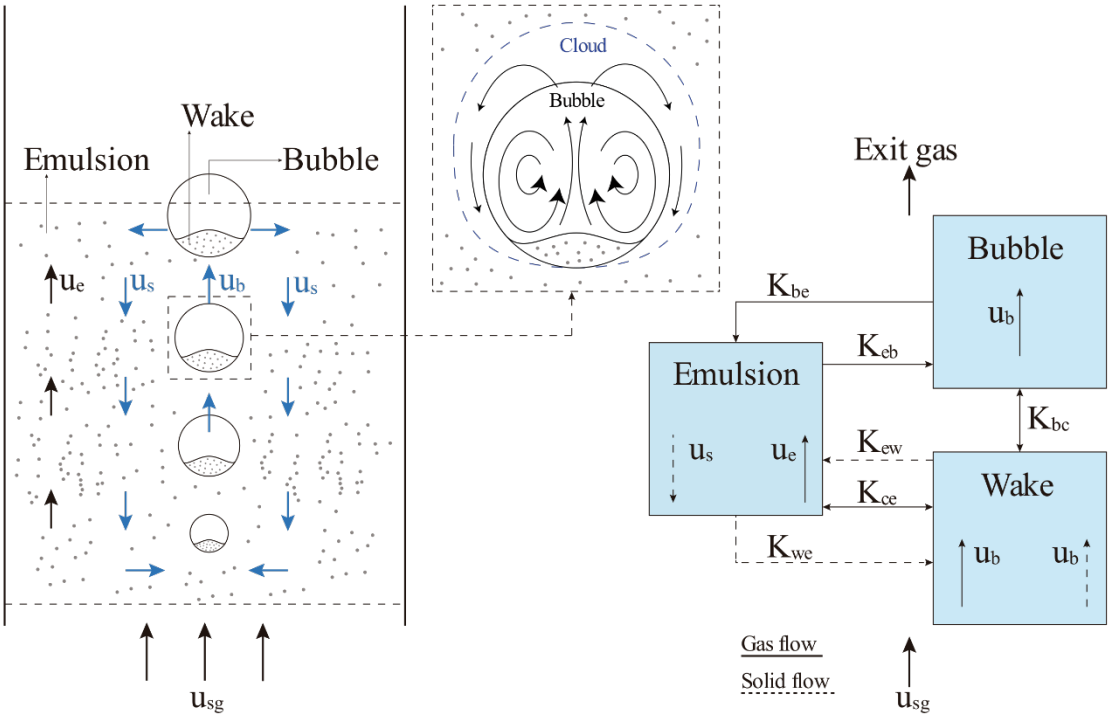

Figure 2. Three-phases model for Fluidized bed reactors

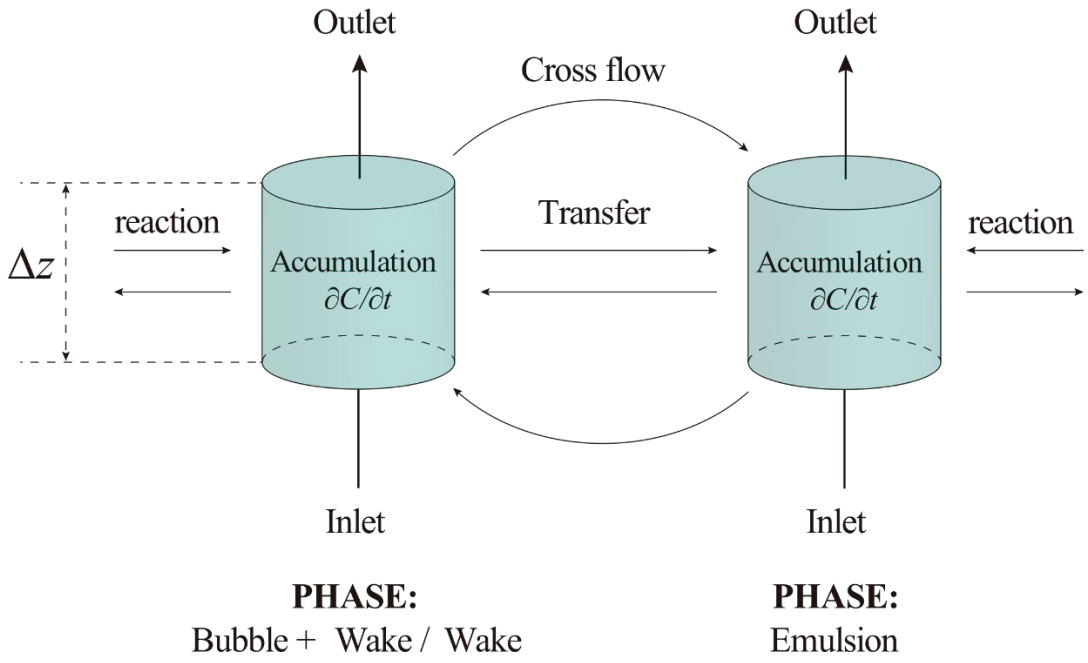

Figure 3. Scheme representing the terms of the mass balances for gases and solid.

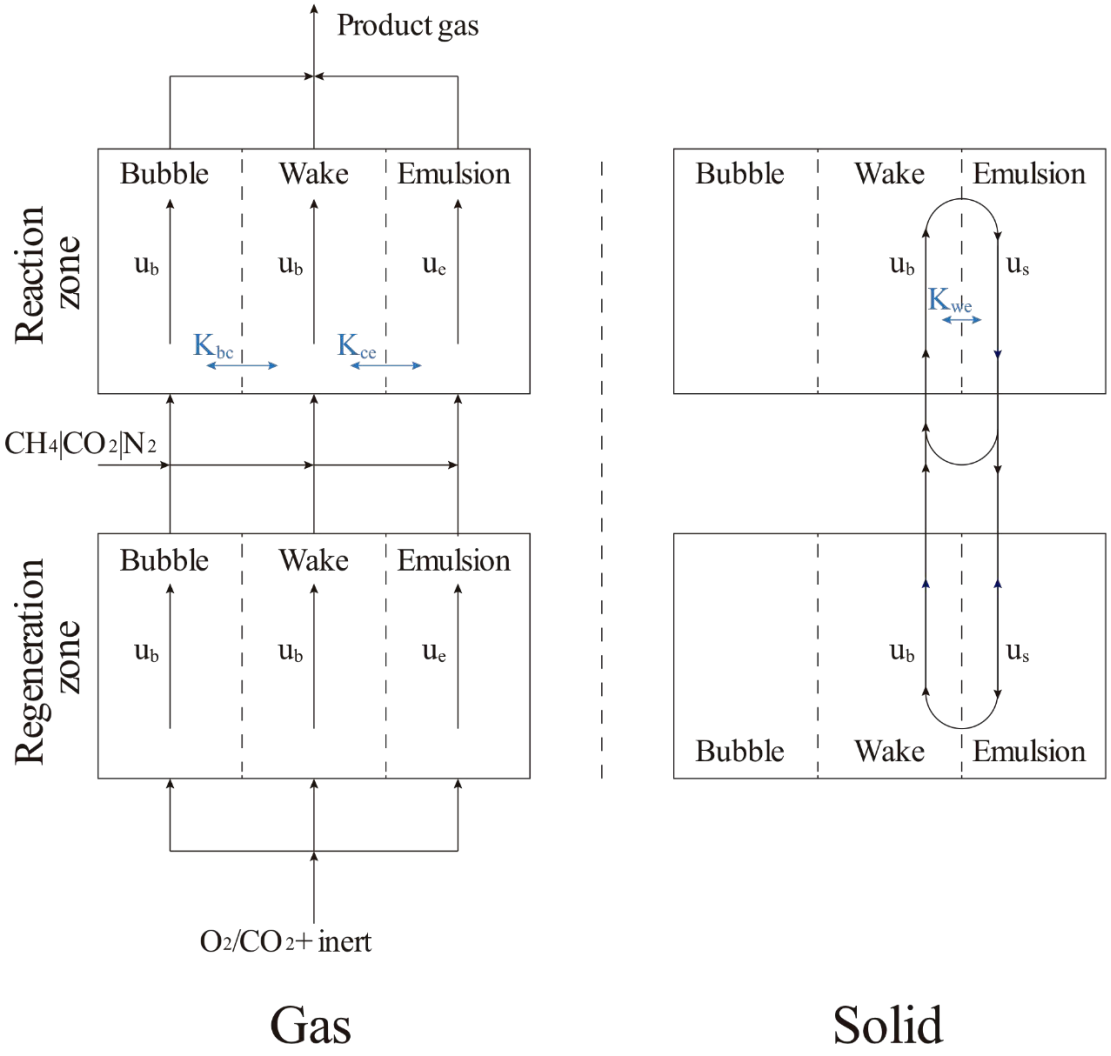

Figure 4. Scheme of the flow model considered for TZFBR/TZFBR+MB

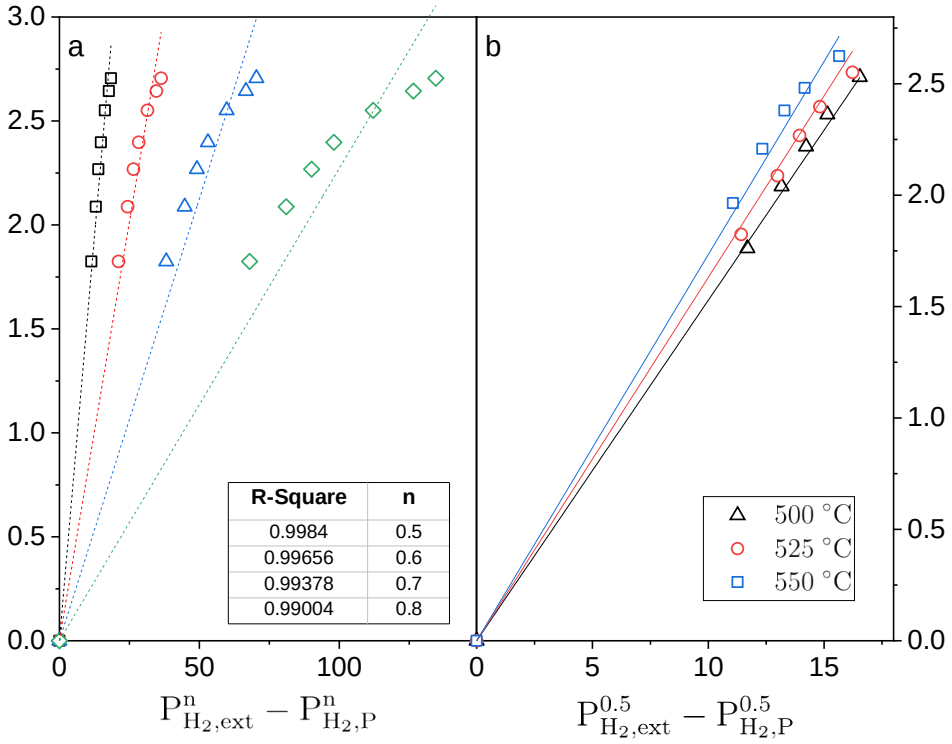

Figure 5 (a) H_2 permeation flux at T = 500 °C for several values of *n*. (b) Effect of temperature on the H_2 permeation flux through a Pd-Ag membrane. In both cases $P_{H2,ext} \approx (P_{H2,F} - P_{H2,R})/\log(P_{H2,F}/P_{H2,R})$.

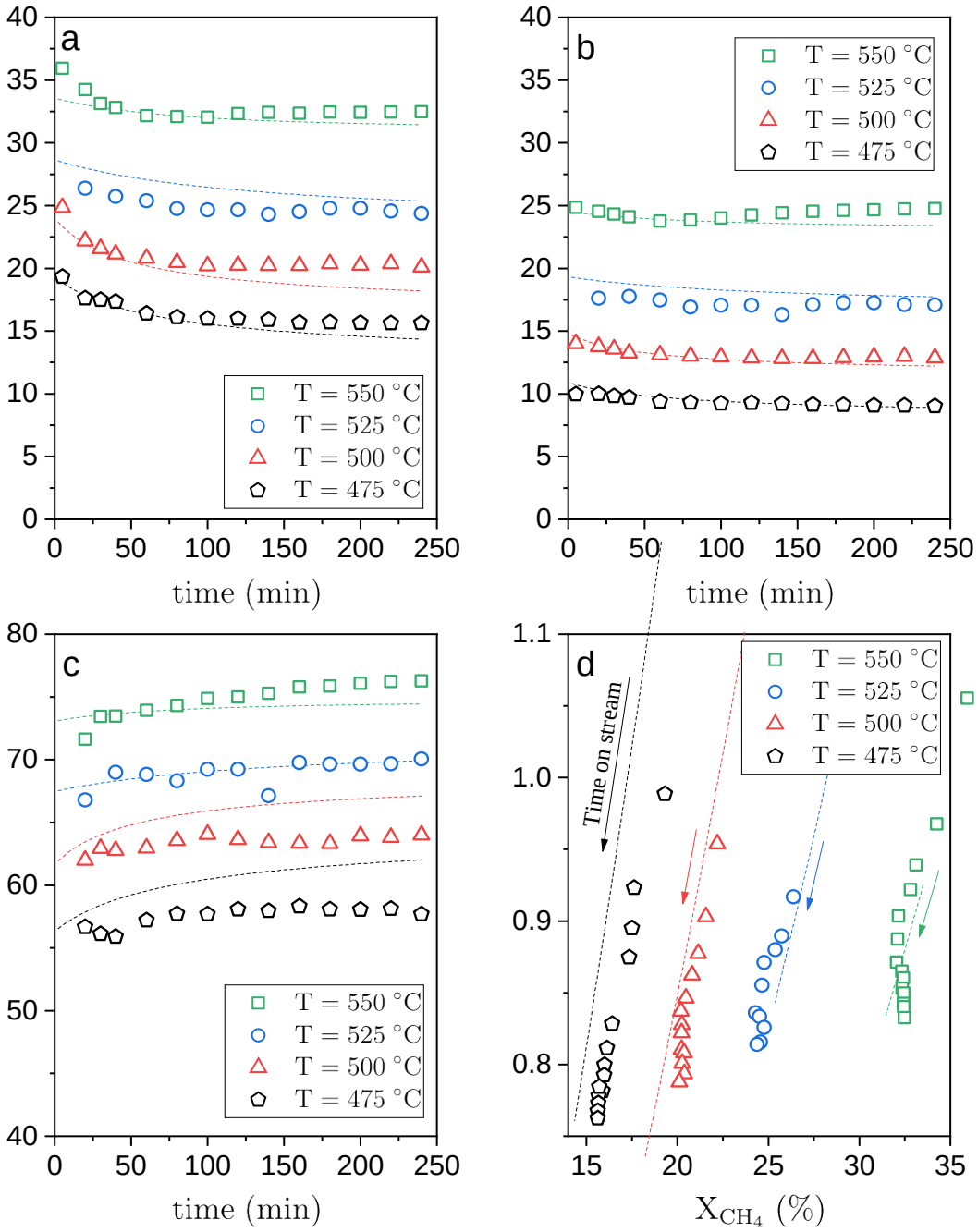

Figure 6. Effect of reaction temperature in CFBR. a) CH_4 conversion. (b) Yield to H_2. (c) Selectivity to H_2. (d) H_2/CO molar ratio. W = 30 g, u_r = 3, $CH_4|CO_2|N_2$ = 40|40|20, time-on-stream = 240 min. Experimental data (symbols), model prediction (lines).

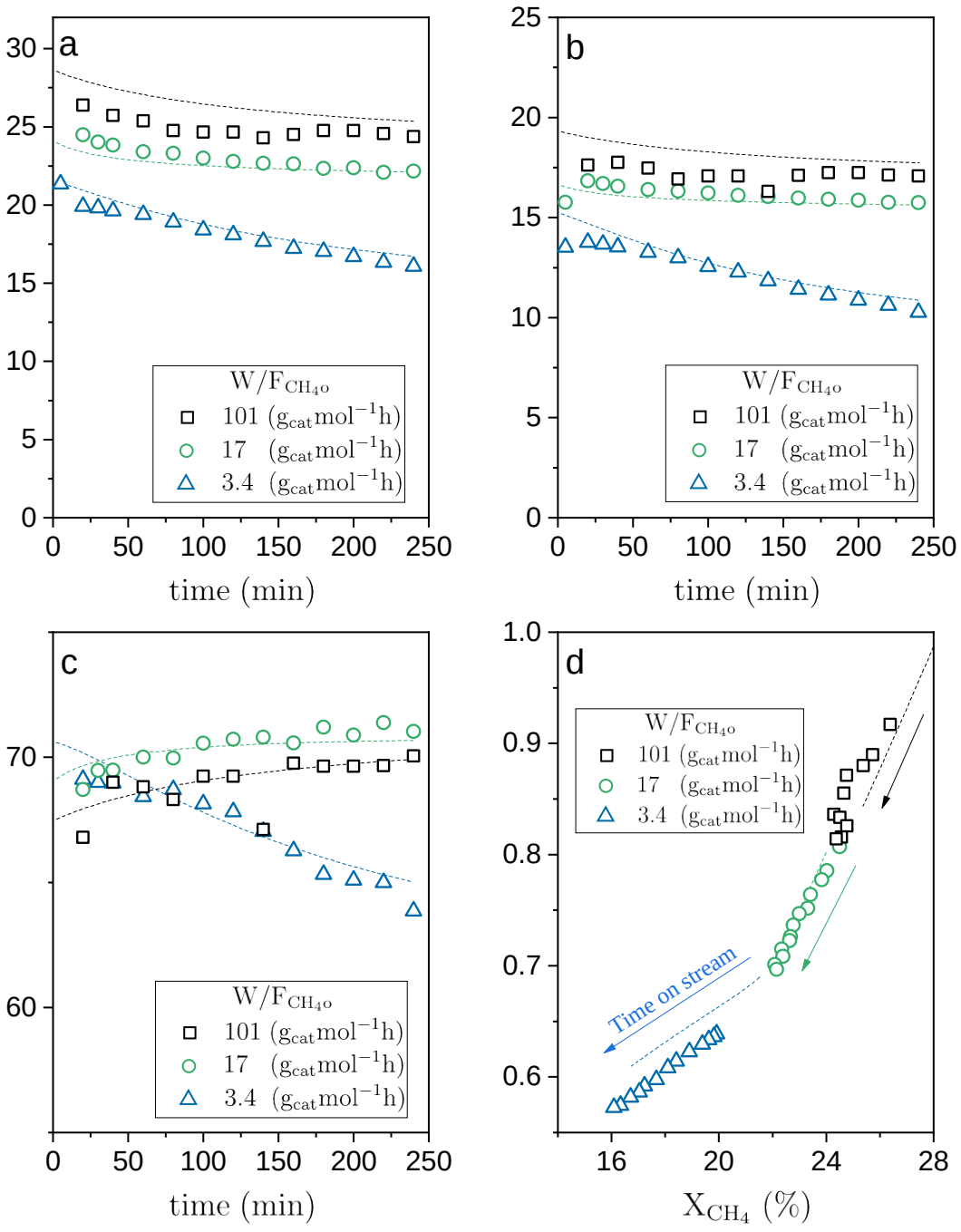

Figure 7. Effect of spatial time in CFBR. (a) CH_4 conversion. (b) Yield to H_2. (c) Selectivity to H_2. (d) H_2/CO molar ratio. T = 525 ºC, u_r = 3, $CH_4|CO_2|N_2$ = 40|40|20, time on stream = 240 min. Experimental data (symbols), model prediction (lines).

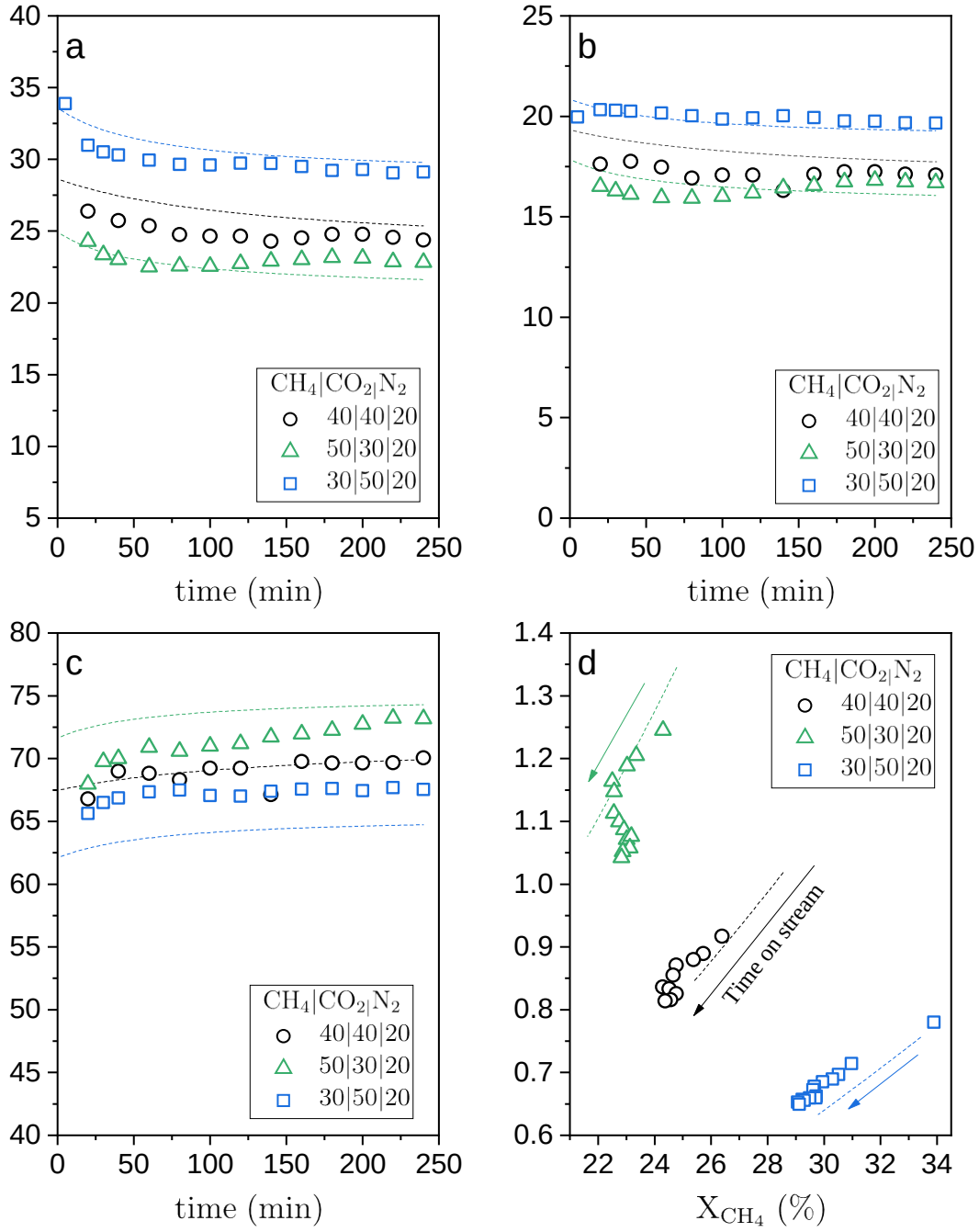

Figure 8. Effect of feed composition in CFBR. (a) CH_4 conversion. (b) Yield to H_2. (c) Selectivity to H_2. (d) H_2/CO molar ratio. T = 525 ºC, u_r = 3, $CH_4|CO_2|N_2$ = 40|40|20, time on stream = 240 min. Experimental data (symbols), model prediction (lines).

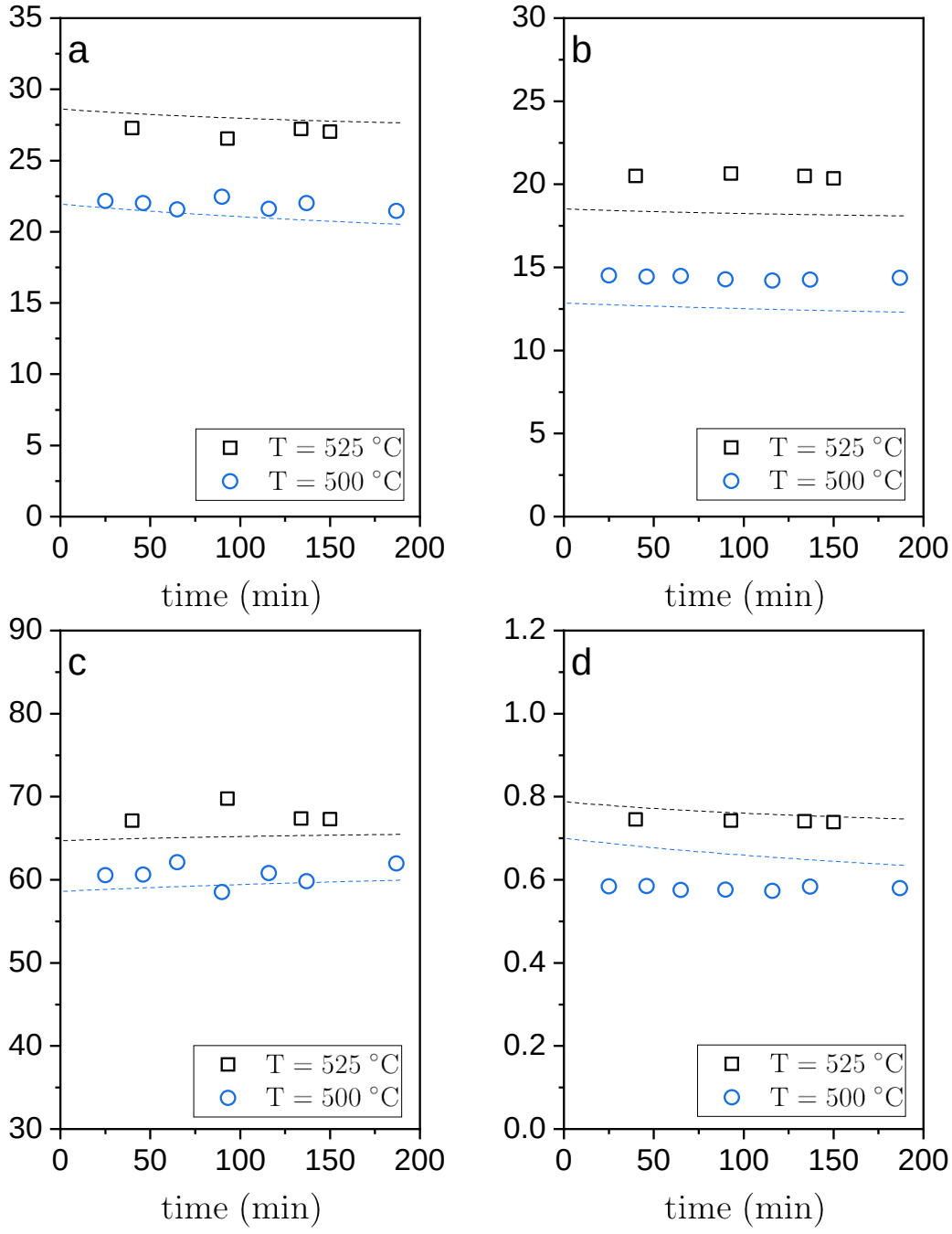

Figure 9. Effect of reaction temperature in a TZFBR. (a) CH_4 conversion. (b) Yield to H_2. (c) Selectivity to H_2. (d) H_2/CO molar ratio. W = 30 g, u_r = 3. Ox = 8% CO_2.. Experimental data (symbols), model prediction (lines).

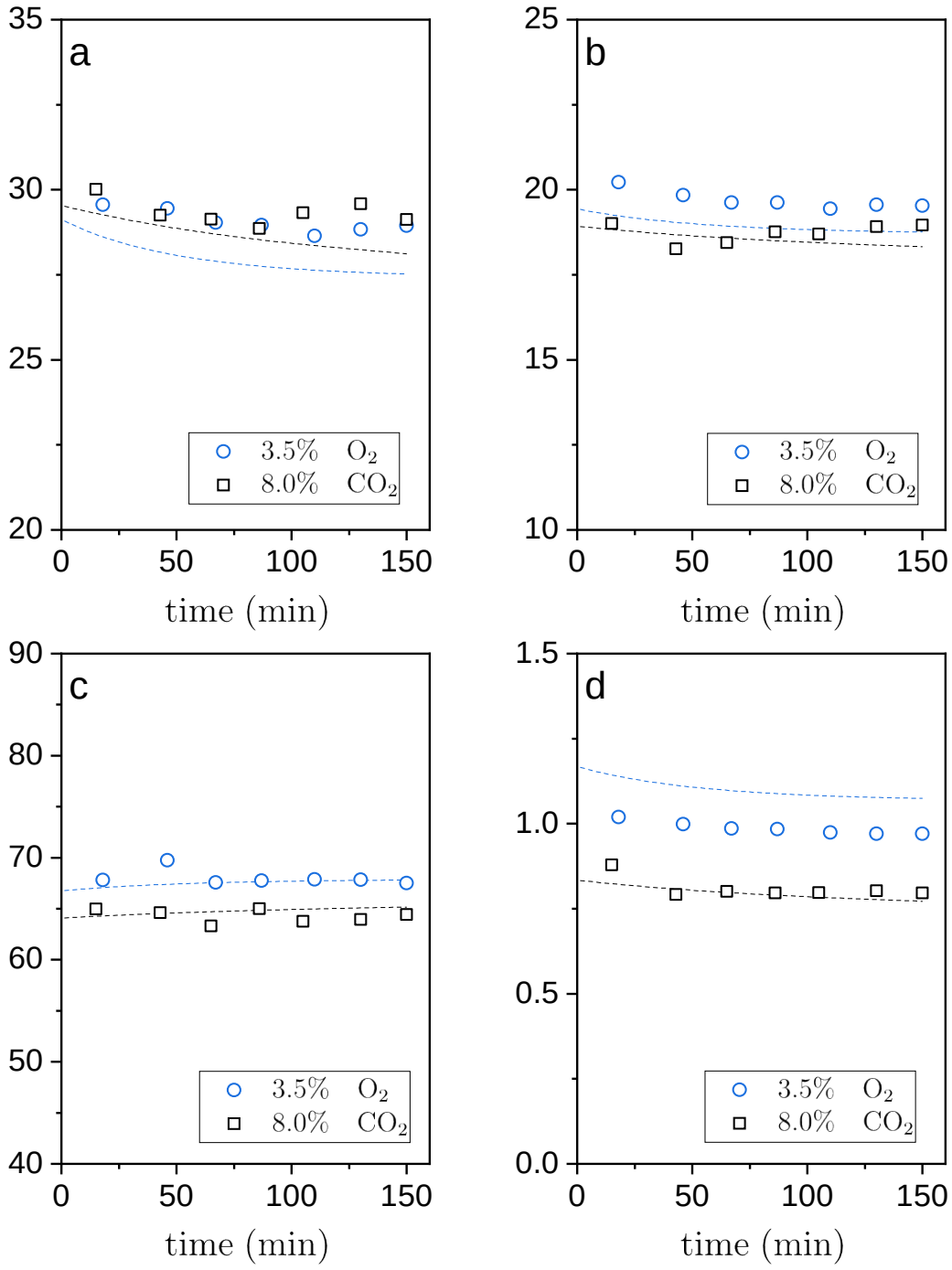

Figure 10. Effect of using O_2 or CO_2 as regenerating gas in a TZFBR. (a) CH_4 conversion. (b) Yield to H_2. (c) Selectivity to H_2. (d) H_2/CO molar ratio. T = 525 ºC. W = 30 g, u_r = 3. W = 30 g, u_r = 3. Ox = 8% CO_2. Experimental data (symbols), model prediction (lines).

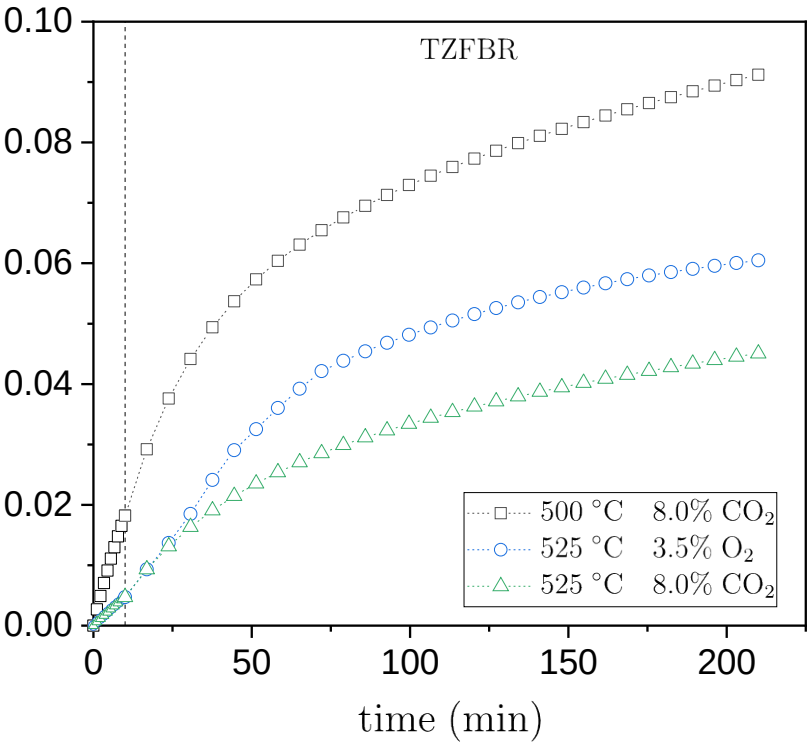

Figure 11. Coke concentration along time-on-stream in a CFBR (stage 1=10 min), TZFBR (stage 2=200 min).

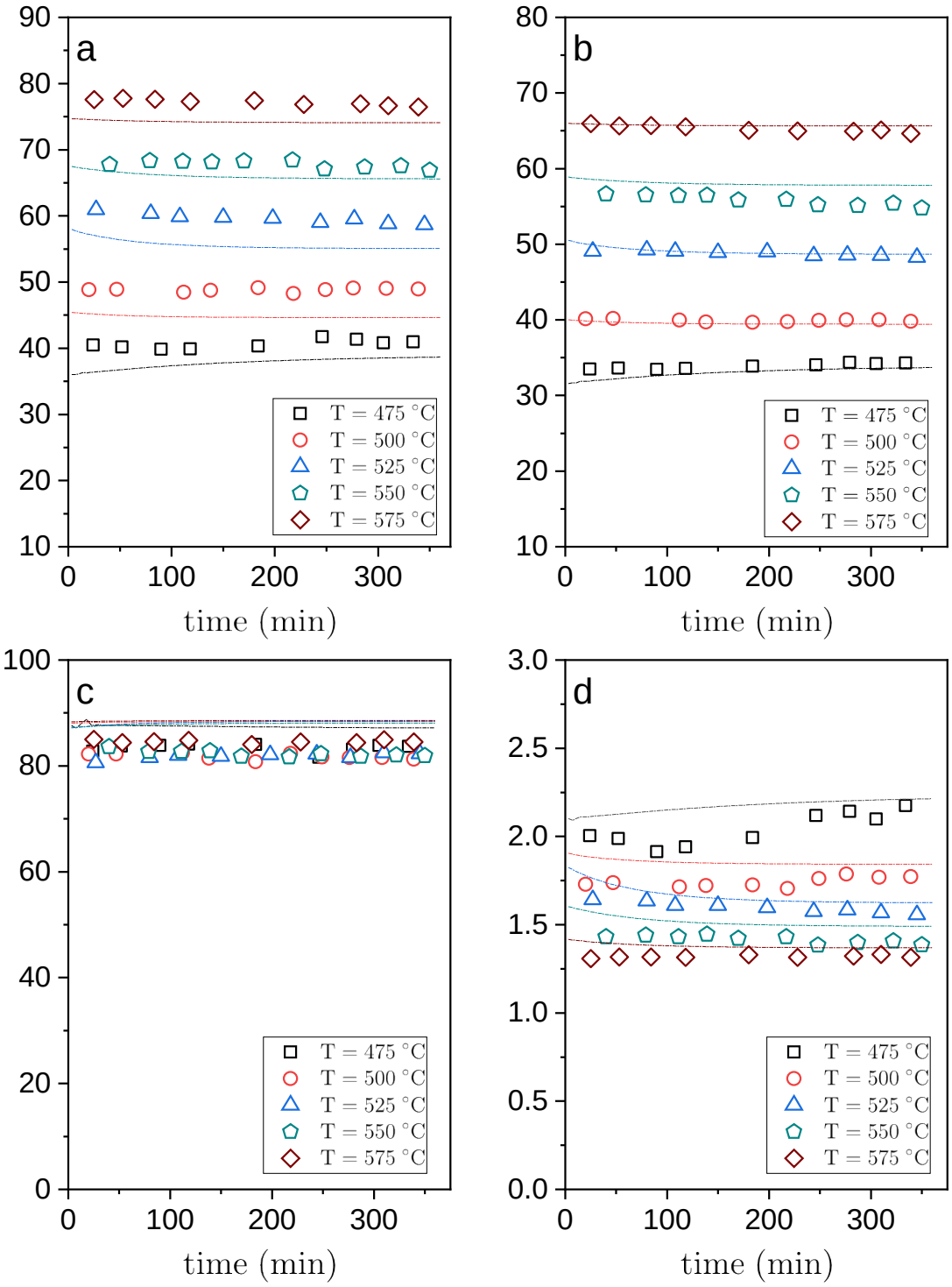

Figure 12. Effect of reaction temperature operating as TZFBR+MB. (a) CH_4 conversion. (b) Yield to H_2. (c) Selectivity to H_2. (d) H_2/CO molar ratio. W = 30 g, u_r = 3. h_f = 2 cm. Experimental data (symbols), model prediction (lines).

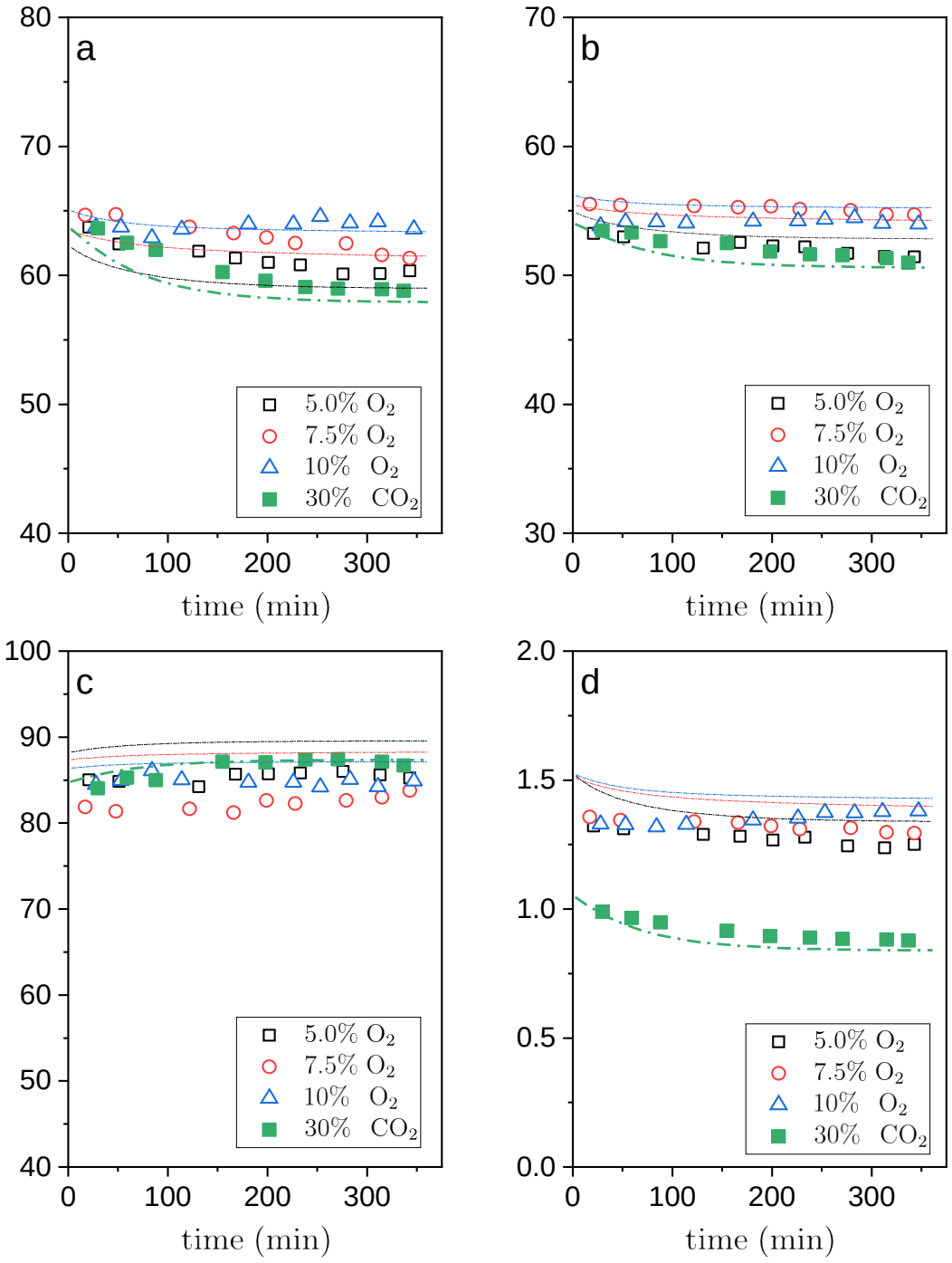

Figure 13. Effect of the amount and nature of regenerating gas in TZFBR+MB. (a) CH_4 conversion. (b) Yield to H_2. (c) Selectivity to H_2. (d) H_2/CO molar ratio. T = 550 °C. W = 30 g, u_r = 3. h_f = 4.5 cm. Experimental data (symbols), model prediction (lines).

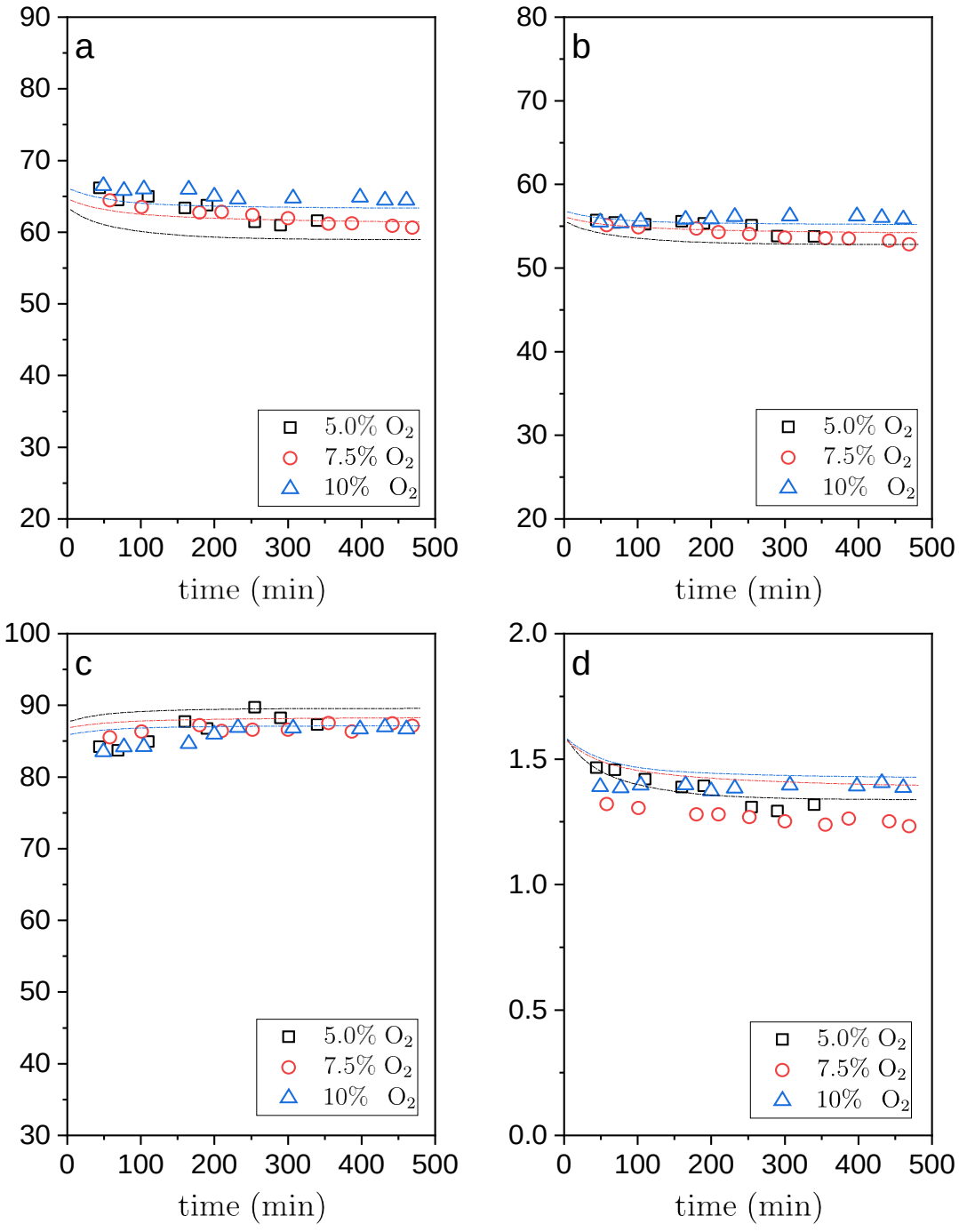

Figure 14.. Results when no activation stage (stage 1) was used in TZFBR+MB. (a) CH_4 conversion. (b) Yield to H_2. (c) Selectivity to H_2. (d) H_2/CO molar ratio. T = 550 °C. W = 30 g, u_r = 3. h_f = 4.5 cm Experimental data (symbols), model prediction (lines).

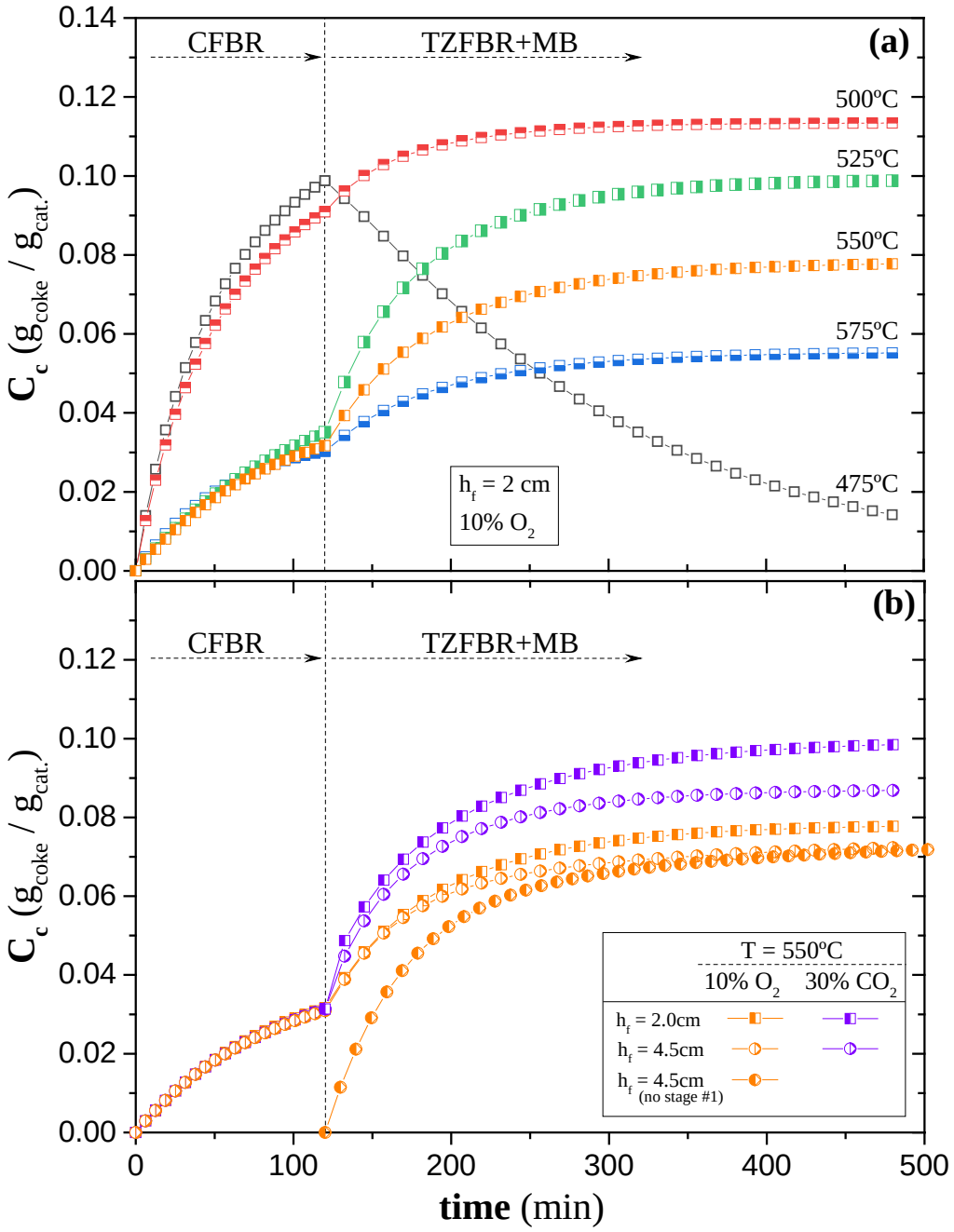

Figure 15. Coke concentration *vs* time-on-stream predicted by the mathematical model at different operating conditions: (a) temperatures, (b) h_f and amount and nature of regenerating gas in TZFBR configuration.